University of Maribor

UNIVERSITY OF THE WEST of SCOTLAND
UWS

10TH International Conference on Sustainable Energy and Environmental Protection:

Marine and Hydro Power

(June 27TH - 30TH, 2017, Bled, Slovenia)

(Conference Proceedings)

Editors:
Emeritus Prof. dr. Jurij Krope
Prof. dr. Abdul Ghani Olabi
Prof. dr. Darko Goričanec
Prof. dr. Stanislav Božičnik

University of Maribor Press


University of Maribor Press

10TH International Conference on Sustainable Energy and Environmental Protection

Marine and Hydro Power

(June 27TH – 30TH, 2017, Bled, Slovenia)

(Conference Proceedings)

Editors:
Emeritus Prof. dr. Jurij Krope
Prof. dr. Abdul Ghani Olabi
Prof. dr. Darko Goričanec
Prof. dr. Stanislav Božičnik

June 2017

Title: 10TH International Conference on Sustainable Energy and Environmental Protection (June 27TH – 30TH, 2017, Bled, Slovenia) (Conference Proceedings)

Subtitle: Marine and Hydro Power

Editors: Emeritus Prof. Jurij Krope, Ph.D. (University of Maribor, Slovenia),
Prof. Abdul Ghani Olabi, Ph.D. (University of the West of Scotland, UK),
Asso. Prof. Darko Goričanec, Ph.D. (University of Maribor, Slovenia),
Asso. Prof. Stanislav Božičnik (University of Maribor, Slovenia).

Review: Prof. Željko Knez, Ph.D. (University of Maribor, Slovenia),
Prof. Niko Samec, Ph.D. (University of Maribor, Slovenia).

Tehnical editors : Jan Perša (University of Maribor Press),
Armin Turanović (University of Maribor Press).

Design and layout: University of Maribor Press

Conference: 10TH International Conference on Sustainable Energy and Environmental Protection

First published in 2017 by
University of Maribor Press
Slomškov trg 15, 2000 Maribor, Slovenia
tel. +386 2 250 42 42, fax +386 2 252 32 45
http://press.um.si, zalozba@um.si

Co-published by
University of Maribor, Faculty of Chemistry and Chemical Engineering
Smetanova ulica 17,2000 Maribor, Slovenia
tel. +386 (0)2 22 94 400, faks + 386 (0)2 25 27 774
http://www.fkkt.um.si, fkkt@um.si

Published: 5. July 2017

CIP - Kataložni zapis o publikaciji
Univerzitetna knjižnica Maribor

621.22:502.174.3(082)(0.034.2)

INTERNATIONAL Conference on Sustainable Energy and Environmental Protection (10 ; 2017 ; Bled)
Marine and hydro power [Elektronski vir] : (Conference proceedings) / 10th International Conference on Sustainable Energy and Environmental Protection, (June 27th-30th, 2017, Bled, Slovenia) ; [organised by] University of Maribor [and] University of the West of Scotland ; editors Jurij Krope ... [et al.]. - El. zbornik. - Maribor : University of Maribor Press, 2017

Način dostopa (URL): http://press.um.si/index.php/ump/catalog/book/246

ISBN 978-961-286-055-4 (pdf)

doi: 10.18690/978-961-286-055-4
1. Gl. stv. nasl. 2. Krope, Jurij 3. Univerza (Maribor)
COBISS.SI-ID 92430337

ISBN 978-961-286-055-4

DOI: https://doi.org/10.18690/978-961-286-055-4

Price: Free copy

For publisher: Prof. Igor Tičar, Ph.D., rector (University of Maribor)

University of Maribor Press

Preface

The 10th International Conference on Sustainable Energy and environmental Protection – SEEP 2017 was organised on June 27th – 30th 2017 in Bled, Slovenia, by:

- Faculty of Chemistry and Chemical Engineering, University of Maribor, Slovenia,
- University of the West of Scotland, School of Engineering and

The aim of SEEP2017 is to bring together the researches within the field of sustainable energy and environmental protection from all over the world.

The contributed papers are grouped in 18 sessions in order to provide access to readers out of 300 contributions prepared by authors from 52 countries.

We thank the distinguished plenary and keynote speakers and chairs who have kindly consented to participate at this conference. We are also grateful to all the authors for their papers and to all committee members.

We believe that scientific results and professional debates shall not only be an incentive for development, but also for making new friendships and possible future scientific development projects.

General chair
Emeritus Prof. dr. Jurij Krope

10TH INTERNATIONAL CONFERENCE ON SUSTAINABLE ENERGY AND ENVIRONMENTAL PROTECTION (JUNE 27TH – 30TH, 2017, BLED, SLOVENIA), MARINE AND HYDRO POWER
J. Krope, A.Ghani Olabi, D. Goričanec & S. Božičnik

University of Maribor Press

Plenary Talk on
The Relation between Renewable Energy and Circular Economy

ABDUL GHANI OLABI - BIBLIOGRAPHY

Prof Olabi is director and founding member of the Institute of Engineering and Energy Technologies (www.uws.ac.uk\ieet) at the University of the West of Scotland. He received his M.Eng and Ph.D. from Dublin City University, since 1984 he worked at SSRC, HIAST, CNR, CRF, DCU and UWS. Prof Olabi has supervised postgraduate research students (10 M.Eng and 30PhD) to successful completion. Prof Olabi has edited 12 proceedings, and has published more than 135 papers in peer-reviewed international journals and about 135 papers in international conferences, in addition to 30 book chapters. In the last 12 months Prof Olabi has patented 2 innovative projects. Prof Olabi is the founder of the International Conference on Sustainable Energy and Environmental Protection SEEP, www.seepconference.co.uk

He is the Subject Editor of the Elsevier Energy Journal https://www.journals.elsevier.com/energy/editorial-board/abdul-ghani-olabi, also Subject editor of the Reference Module in Materials Science and Materials Engineering http://scitechconnect.elsevier.com/reference-module-material-science/ and board member of a few other journals. Prof Olabi has coordinated different National, EU and International Projects. He has produced different reports to the Irish Gov. regarding: Hydrogen and Fuel Cells and Solar Energy.

CORRESPONDENCE ADDRESS: Abdul Ghani Olabi, Ph.D., Professor, University of the West of Scotland, School of Engineering and Computing, D163a, McLachlan Building, Paisley, United Kingdom, e-mail: Abdul.Olabi@uws.ac.uk.

https://doi.org/10.18690/978-961-286-055-4 ISBN 978-961-286-055-4

Available at: http://press.um.si.

10TH INTERNATIONAL CONFERENCE ON SUSTAINABLE ENERGY AND ENVIRONMENTAL PROTECTION (JUNE 27TH – 30TH, 2017, BLED, SLOVENIA), MARINE AND HYDRO POWER
J. Krope, A.Ghani Olabi, D. Goričanec & S. Božičnik

University of Maribor Press

Plenary Talk on Energy Footprints Reduction and Virtual Footprints Interactions

JIŘÍ JAROMÍR KLEMEŠ & PETAR SABEV VARBANOV

Increasing efforts and resources have been devoted to research during environmental studies, including the assessment of various harmful impacts from industrial, civic, business, transportation and other economy activities. Environmental impacts are usually quantified through Life Cycle Assessment (LCA). In recent years, footprints have emerged as efficient and useful indicators to use within LCA. The footprint assessment techniques has provided a set of tools enabling the evaluation of Greenhouse Gas (GHG) – including CO_2, emissions and the corresponding effective flows on the world scale. From all such indicators, the energy footprint represents the area of forest that would be required to absorb the GHG emissions resulting from the energy consumption required for a certain activity, excluding the proportion absorbed by the oceans, and the area occupied by hydroelectric dams and reservoirs for hydropower.

An overview of the virtual GHG flow trends in the international trade, associating the GHG and water footprints with the consumption of goods and services is performed. Several important indications have been obtained: (a) There are significant GHG gaps between producer's and consumer's emissions – US and EU have high absolute net imports GHG budget. (b) China is an exporting country and increasingly carries a load of GHG emission and virtual water export associated with consumption in the relevant importing countries. (c) International trade can reduce global environmental pressure by redirecting import to products produced with lower intensity of GHG emissions and lower water footprints, or producing them domestically.

To develop self-sufficient regions based on more efficient processes by combining neighbouring countries can be a promising development. A future direction should be focused on two main areas: (1) To provide the self-sufficient regions based on more efficient processes by combining production of surrounding countries. (2) To develop the shared mechanism and market share of virtual carbon between trading partners regionally and internationally.

CORRESPONDENCE ADDRESS: Jiří Jaromír Klemeš, DSc, Professor, Brno University of Technology - VUT Brno, Faculty of Mechanical Engineering, NETME Centre, Sustainable Process Integration Laboratory – SPIL, Technická 2896/2, 616 69 Brno, Czech Republic, e-mail: klemes@fme.vutbr.cz. Petar Sabev Varbanov, Ph.D., Associate Professor, Brno University of Technology - VUT Brno, Faculty of Mechanical Engineering, NETME Centre, Sustainable Process Integration Laboratory – SPIL, Technická 2896/2, 616 69 Brno, Czech Republic, e-mail: varbanov@fme.vutbr.cz.

https://doi.org/10.18690/978-961-286-055-4 ISBN 978-961-286-055-4

Available at: http://press.um.si.

University of Maribor Press

JIŘÍ JAROMÍR KLEMEŠ - BIBLIOGRAPHY

Head of "Sustainable Process Integration Laboratory – SPIL", NETME Centre, Faculty of Mechanical Engineering, Brno University of Technology - VUT Brno, Czech Republic and Emeritus Professor at "Centre for Process Systems Engineering and Sustainability", Pázmány Péter Catholic University, Budapest, Hungary.

Previously the Project Director, Senior Project Officer and Hon Reader at Department of Process Integration at UMIST, The University of Manchester and University of Edinburgh, UK. Founder and a long term Head of the Centre for Process Integration and Intensification – CPI2, University of Pannonia, Veszprém, Hungary. Awarded by the EC with Marie Curies Chair of Excellence (EXC). Track record of managing and coordinating 91 major EC, NATO and UK Know-How projects. Research funding attracted over 21 M€.

Co-Editor-in-Chief of Journal of Cleaner Production (IF=4.959). The founder and President for 20 y of PRES (Process Integration for Energy Saving and Pollution Reduction) conferences. Chairperson of CAPE Working Party of EFCE, a member of WP on Process Intensification and of the EFCE Sustainability platform.

He authored nearly 400 papers, h-index 40. A number of books published by McGraw-Hill; Woodhead; Elsevier; Ashgate Publishing Cambridge; Springer; WILEY-VCH; Taylor & Francis).

Several times Distinguished Visiting Professor for Universiti Teknologi Malaysia, Xi'an Jiaotong University; South China University of Technology, Guangzhou; Tianjin University in China; University of Maribor, Slovenia; University Technology Petronas, Malaysia; Brno University of Technology and the Russian Mendeleev University of Chemical Technology, Moscow. Doctor Honoris Causa of Kharkiv National University "Kharkiv Polytechnic Institute" in Ukraine, the University of Maribor in Slovenia, University POLITEHNICA Bucharest, Romania. "Honorary Doctor of Engineering Universiti Teknologi Malaysia", "Honorary Membership of Czech Society of Chemical Engineering", "European Federation of Chemical Engineering (EFCE) Life-Time Achievements Award" and "Pro Universitaire Pannonica" Gold Medal.

CORRESPONDENCE ADDRESS: Jiří Jaromír Klemeš, DSc, Professor, Brno University of Technology - VUT Brno, Faculty of Mechanical Engineering, NETME Centre, Sustainable Process Integration Laboratory – SPIL, Technická 2896/2, 616 69 Brno, Czech Republic, e-mail: klemes@fme.vutbr.cz.

https://doi.org/10.18690/978-961-286-055-4 ISBN 978-961-286-055-4

Available at: http://press.um.si.

10TH INTERNATIONAL CONFERENCE ON SUSTAINABLE ENERGY AND ENVIRONMENTAL PROTECTION (JUNE 27TH – 30TH, 2017, BLED, SLOVENIA), MARINE AND HYDRO POWER
J. Krope, A.Ghani Olabi, D. Goričanec & S. Božičnik

Plenary Talk on
Renewable energy sources for environmental protection

HAKAN SERHAD SOYHAN

Development in energy sector, technological advancements, production and consumption amounts in the countries and environmental awareness give shape to industry of energy. When the dependency is taken into account in terms of natural resources and energy, there are many risks for countries having no fossil energy sources. Renewable and clean sources of energy and optimal use of these resources minimize environmental impacts, produce minimum secondary wastes and are sustainable based on current and future economic and social societal needs. Sun is one of the main energy sources in recent years. Light and heat of sun are used in many ways to renewable energy. Other commonly used are biomass and wind energy. To be able to use these sources efficiently national energy and natural resources policies should be evaluated together with the global developments and they should be compatible with technological improvements. Strategic plans with regard to energy are needed more intensively and they must be in the qualification of a road map, taking into account the developments related to natural resources and energy, its specific needs and defining the sources owned by countries. In this presentation, the role of supply security was evaluated in term of energy policies. In this talk, new technologies in renewable energy production will be shown and the importance of supply security in strategic energy plan will be explained.

CORRESPONDENCE ADDRESS: Hakan Serhad Soyhan, Ph.D., Professor, Sakarya University, Engineering Faculty, Esentepe Campus, M7 Building, 54187 - Esentepe /Sakarya, Turkey, e-mail: hsoyhan@sakarya.edu.tr.

https://doi.org/10.18690/978-961-286-055-4 ISBN 978-961-286-055-4

Available at: http://press.um.si.

University of Maribor Press

HAKAN SERHAD SOYHAN - BIBLIOGRAPHY

Professor at Sakarya University, Engineering Faculty. 50 % fot teaching and the rest for reasearch activities.

Teaching, courses taught:

Graduate courses:

- Combustion technology;
- Modelling techniques;

Undergraduate courses:

- Combustion techniques;
- Internal combustion engines;
- Fire safety.

Tehnical skills and competences professional societies:

- 25 jurnal papers in SCI Index. 23 conference papers;
- Editor at FCE journal. Co-editor at J of Sakarya University;
- Head of Local Energy Research Society (YETA);
- Member od American Society of Mechanical engineers (ASME);
- Member of Turkish Society of Mechanical Engineers (TSME).

CORRESPONDENCE ADDRESS: Hakan Serhad Soyhan, Ph.D., Professor, Sakarya University, Engineering Faculty, Esentepe Campus, M7 Building, 54187 - Esentepe /Sakarya, Turkey, e-mail: hsoyhan@sakarya.edu.tr.

https://doi.org/10.18690/978-961-286-055-4 ISBN 978-961-286-055-4

Available at: http://press.um.si.

University of Maribor Press

Table of Contents

CONFERENCE PROCEEDINGS

10TH INTERNATIONAL CONFERENCE ON SUSTAINABLE ENERGY AND ENVIRONMENTAL PROTECTION (JUNE 27TH – 30TH, 2017, BLED, SLOVENIA), MARINE AND HYDRO POWER
J. Krope, A.Ghani Olabi, D. Goričanec & S. Božičnik

Fuzzy Logic Based Complex System Control Implementation on Wave Energy Converters

ALPER BURGAÇ & HAKAN YAVUZ

Abstract This study presents the results of the Fuzzy Logic (FL) based control application for heaving type wave energy converter (WEC) operating in realistic sea state conditions. It has been shown in literature that the power capture performance of heaving WECs depends on the resonance with incident the wave frequency. In regular sea wave conditions, the task of setting the control parameters for sinusoidal waves is a well-known easy task if the wave frequency is known. However, in realistic sea conditions, the wave frequency needed for control settings is not clearly defined One of the approaches proposed in literature is to use of dominant wave frequency. This dominant wave frequency can be estimated by a model using the Discrete Fourier Transform approach. The presented model utilizes the estimated wave frequency in FL controller for determination of the PTO control settings. This approach not only uses PTO based for the fast tuning technique, but also introduces slow tuning method. As a part of the study, the developed realistic simulation model and proposed FL based controller is used to combine the fast and slow tuning techniques. The simulation results for realistic sea conditions are presented.

Keywords: • Renewable energy • wave energy converter • wave power • control • fuzzy logic •

CORRESPONDENCE ADDRESS: Alper Burgaç, Ph.D., Assistant, Çukurova University, Engineering and Architecture Faculty, Çukurova Üniversitesi Rektörlüğü, 01330 Sarıçam, Adana, Turkey, e-mail: alperburgac@cu.edu.tr. alperburgac@yahoo.com. Hakan Yavuz, Ph.D., Professor, Çukurova University, Engineering and Architecture Faculty, Çukurova Üniversitesi Rektörlüğü, 01330 Sarıçam, Adana, Turkey, e-mail: dr.hakanyavuz@gmail.com.

https://doi.org/10.18690/978-961-286-055-4.1 ISBN 978-961-286-055-4

Available at: http://press.um.si.

1 Introduction

With the advance of the technology in our daily life, the need for energy increases every day. The increasing demand for higher energy and also the environmental concerns lead to search for environmentally friendly energy sources. The main environmentally friendly renewable sources of energy are wind, solar and wave energy. These renewable energy sources are mostly utilised or the related technology has reached to a certain level of capacity for wind and solar systems. However, the developments for wave energy based power systems seem to be slower in development relative to the other two renewable energy sources. [1]

Wave energy converter (WEC) is a device that converts energy of incoming waves into electrical power which is then supplied to the grid. The configuration of the WECs vary according to many aspects, that is, the installation site (i.e., on-shore, near-shore or offshore), the principle of operation (i.e., oscillating, pitching, surging etc.) and the deployed power take-off (PTO) mechanisms. The economic feasibility of the WEC appears to depend on the wave potential at the installation site, the efficiency of the PTO system, and the effectiveness of the control strategy used, along with other factors such as installation and maintenance costs [2].

The oceans have been reported to have great wave energy potential [3]. However, the irregular nature of ocean waves and complexity of wave-WEC interaction makes the issue a challenging one [4]. Although, control techniques appear to improve the wave power extraction potential, understanding of the overall issue still remains to be weak. One of the main challenges in offshore systems development is to apply the control techniques to WECs. The control strategies for oscillating types mainly aim keeping the WECs at resonance by adjusting the WEC natural frequency to match the incident wave frequency [1]. There are a number of studies presents details on development of control systems for WECs [5,6,7]. The optimum control of wave energy converters is discussed in detail by Falnes [8], where almost all aspects of control and related tuning methods are summarized in a framework that outlines and covers various tuning methods [4,8,9]. Another issue for control is to adjust control parameters in realistic wave conditions. In simple terms, the task of tuning of a WEC is achieved by adjusting the Power-Take- Off System (PTOS) settings to the right values at the right time [9]. This paper presents results for tuning WEC parameters with both slow and fast tuning methods to make the control approach more realistic and practical. There will be three different cases of analyses use for the comparison of the power capture performances. In the first case (Case 1), only instantaneously adjustable stiffness and damping based tuning is assumed. In the second case (Case 2), quantized version of stiffness along with instantaneous damping is used. In the final case (Case 3), quantized version of stiffness along with instantaneous damping is supported by FL based slow tuning where an on-board water tank and related water storage quantity is used in manipulation of the overall system mass.

2 Fuzzy logic control

The term fuzzy logic was first introduced in 1965 by Lotfi Zadeh [10,11]. (FL) controllers have been used to handle complex systems where system parameters have an inherit uncertainty. This is defined as the concept of partial truth, where the truth value may range between completely true and completely false [12].

Especially for the case of wave energy converters, system parameters contain high level of uncertainty. For such control applications where system parameters contain uncertainty, the control problem becomes a really complicated issue. This is where FL control systems become an important tools for development of controllers for WECs as FL controllers are capable of handling uncertainty very well.

The main issue in use of the FL controller design is to define the rule base. That has been some papers in literature on FL control applications based on WEC control [2,6,13]. In most of the reported cases of FL controllers, the research is focused on use of a controller for power take-off settings. In most of the cases reported in literature, the damping and stiffness settings appear to be the only parameters being determined by the FL controller [2].

In our case, FL controller is used in adjustment of the added mass for the water tank of the wave energy converter for slow tuning.

3 Mathematical Model

The heaving WEC studied in this paper has been described in [1] where all necessary details are provided. In order to avoid repetition (mostly covering Case 1), those details are not provided here. As illustrated in Figure 1, the Time-Domain model of the point-absorber WEC system [1,14] consists of two parts that run in consecutive steps. In the wave force pre-processing part of the simulation, the time-series wave elevation data is processed to yield the time-series wave force signal, and the time-series wave frequency signal is also estimated. The power conversion part is, on the other hand, based on a MATLAB/SIMULINK™ [15] model, where the wave force is used to excite the WEC model and the displacement (x) and velocity (v) signals are calculated. These signals, along with k_{pto} and b_{pto}, are then used in PTO where the instantaneous power (P_{ins}), moving average power (P_{ma}) and the controlled force (H) are calculated. The controller block in Figure 1 uses the estimated wave frequency signal and generates the optimum PTO settings (k_{pto}, b_{pto}) using the ideal point-absorber WEC theory. It also calculates the necessary added mass m_{st} for the water tank for slow tuning. The below model describes the operation of Case 1 and Case 2 if considering controller only using

PTO settings for control without m_{st}. In the third case (Case 3), the controller uses the PTO settings and m_{st} for controlling the operation of the WEC.

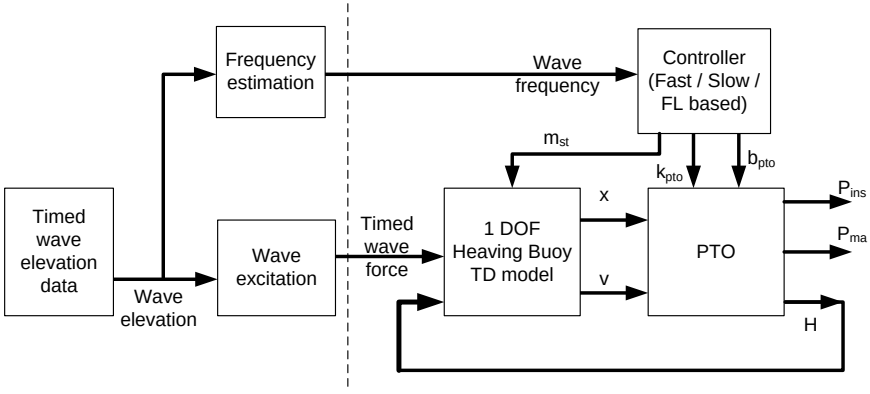

Figure 1. Overall model of the point-absorber WEC system

The equation of motion in the time domain for a single translation mode, or degree of freedom, subject to wave effects can be expressed in the form

$$m_{dry}\ddot{x}(t) = F(t) \tag{1}$$

in which $x(t)$ is the position of the body at time t, m_{dry} represents the inertial mass of the body, a represents added mass and $F(t)$ is the total force on the body. Eq. (1) can be expressed below

$$(m_{dry}+a)\ddot{x}(t)+b\dot{x}(t)+cx(t)+\int_{-\infty}^{t} K_R+(t-\tau)\dot{x}(\tau)d\tau = \int_{-\infty}^{+\infty} K_E(t-\tau)\zeta(\tau)d\tau - H(t) \tag{2}$$

With zero initial conditions (i.e. at 'rest'), it can also be shown [4 and 5] that the Laplace transform of Eq. (2) can take the form

$$[(m_{dry}+a)s^2+bs+c]X(s)+\frac{B_R(s)}{A_R(s)}sX(s) = \frac{B_E(s)}{A_E(s)}Z(s)-H(s) \tag{3}$$

where $X(s)$, $Z(s)$ and $H(s)$ are the Laplace transforms of $x(t)$, $\zeta(t)$ and $H(t)$ respectively.

The above mathematical model describes the WEC operated in Case 1 and Case 2. However in Case 3, the overall mass of the system is varied with settings provided from the controller. In this case, the overall mass of the system (M) can be described by the below equation.

$$M = m_{dry} + a + m_{tnk} + m_{st} \tag{4}$$

Further details on DFT analysis of wave elevation for wave information generation, wave force calculation, approach used in determination of PTO settings, calculation of instantaneous power (P_{ins}) and moving average power (P_{ma}) can be found in the study presented in [1].

4 Simulation studies

Most WECs control studies assume instantaneous variation of PTO settings for control applications. However, in practice instantaneous achievement of PTO settings may not be practical due to response time of such mechanical systems. It is also worth mentioning that such applications may require high levels of power to achieve instantaneous and accurate control of settings. It is also necessary to assess the cost of instantaneous variation of parameters and to provide a solution to this problem. In Case 1 the control parameters are varied instantly. In Case 2, the stiffness is quantized while damping is still instantaneously varied. In final case (Case 3), to compensate for the losses of quantized level of stiffness added mass parameter (m_{st}) is used for slow tuning thereby improving the system power capture performance. In this approach as a part of slow tuning an on-board water tank and related water storage quantity is used in manipulation of the overall system mass to manipulate the system's natural frequency. Hence, in this case the tuning of the WEC is achieved by both slow and fast tuning methods to make the control approach more realistic and practical.

4.1 Case1:Achievement of instantaneous k_{pto} with a servo hydraulic system

In In this case, the control approach is based on instantaneous adjustment of stiffness parameter of power take off (PTO) unit for wave energy converters (WEC). The control parameters are used to get resonant motion for maximized the energy production. But there are some practical problems such as varying the k_{pto} parameter instantly. The main issue here is such fast achievement of stiffness settings. Assuming that it is technically possible to achieve such a speed, the necessary power to achieve this may be too high.

The double acting hydraulic cylinder mechanism is selected to achieve instantaneous adjustment of PTO stiffness (k_{pto}). To achieve the required stiffness and related force, the hydraulic cylinder is used directly. The F_{kpto} is calculated as in Eq. (10) below:

$$F_{kpto} = k_{pto} x \tag{10}$$

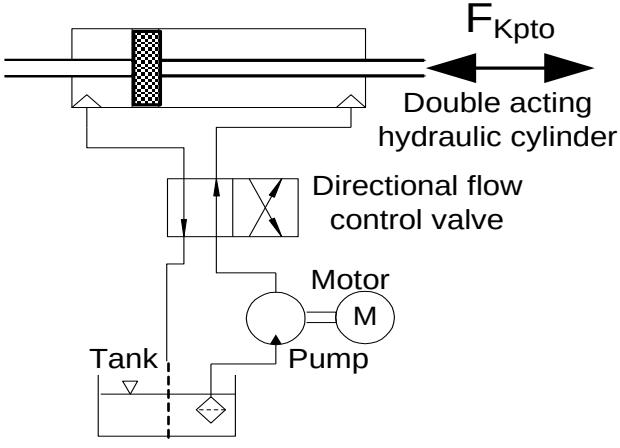

Figure 2. The outline of the instantaneous k_{pto} setting achievement using a hydraulic system

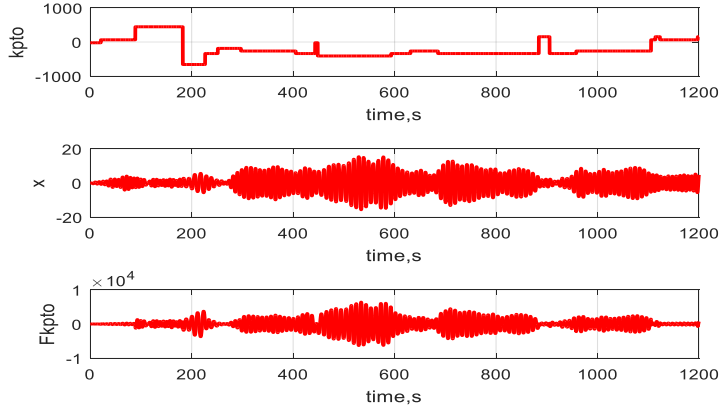

Figure 3. k_{pto} settings, displacement and related F_{kpto} for case 1

In Figure 3, settings for k_{pto} are provided for a realistic sea state. In the figure also the displacement and the force required for achievement of k_{pto} is presented. In Figure 4, Hydraulic Pressure (P_{hyd}), flow rate and hydraulic power (P_{hyd}) required for instantaneous achievement of k_{pto} and required electrical power (P_{elec}) for Case 1.The power results for Case 1 are given in Figure 4 and Figure 5. The Figure 5 shows the instantenous power (P_{ins}) and moving average power (P_{ma})produced with instantaneous settings. As simulation result, total captured power is calculated as 572 kW . In Figure 6, the power requirement for stiffness, power capture performance and related power levels are illustrated. It can be seen that the power required for instantaneous achievement of PTO settings require much more power than the device actually captures.

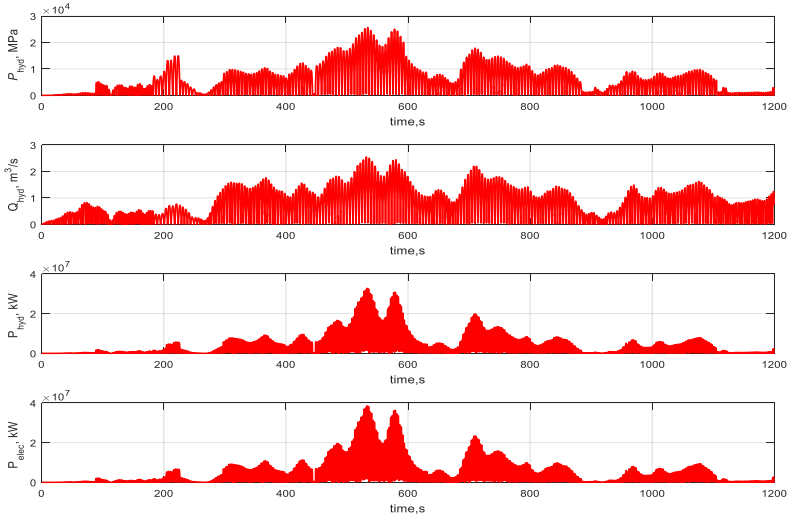

Figure 4. Hydraulic Pressure, flow rate and hydraulic power required for instantaneous k_{pto} achievement and required electrical power for Case 1

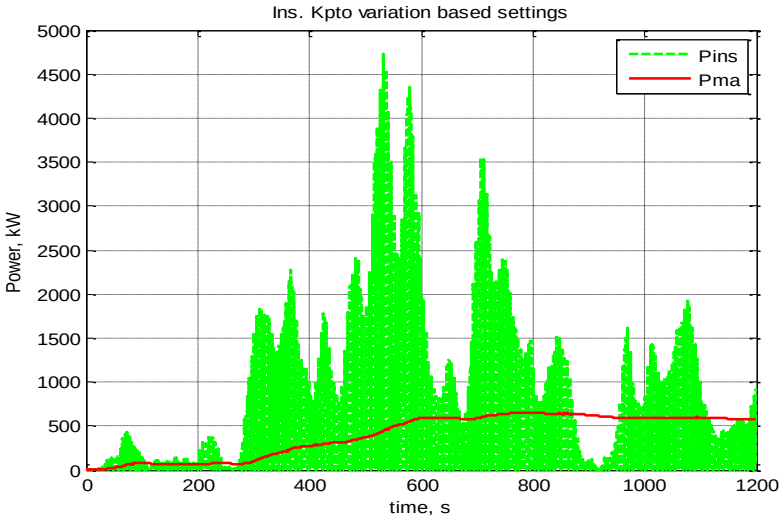

Figure 5. Produced power for Case 1

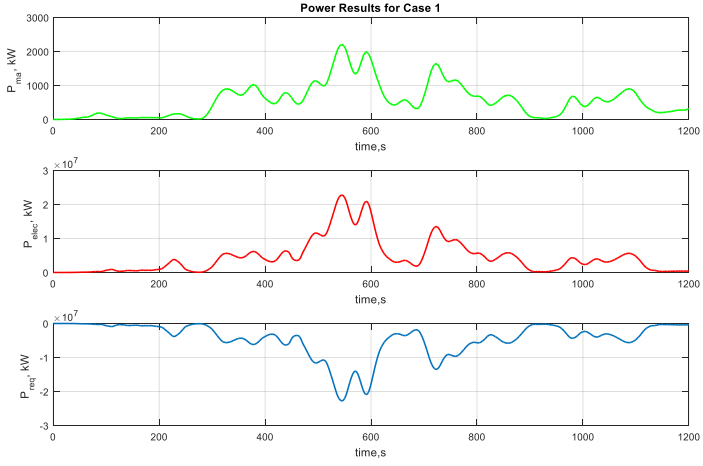

Figure 6. Power results for Case 1

4.2 Case2:Achievement of quantized k_{pto}

In this case, PTO stiffness is quantized. For this purpose, the control parameters for instantaneous parameter change are given in the table below. From this table the minimum and maximum values of stiffness settings are determined. These results are used in quantization of the tuning parameters. For quantization of stiffness, 16 springs

are used and this makes 8 quantization levels considering symmetric positioning of springs in the system. Each symmetric couple of springs set are activated by a hydraulic cylinder pushing the springs into action while releasing when they are not in use.

Table 1: Maximum and minimum required k_{pto} values

#Dataset No	k_{pto}^{min} (kN/m)	k_{pto}^{max} (kN/m)
1	-657,86	661,26
2	-657,86	450,2
3	-474,83	-103,83
4	-539,14	67,65

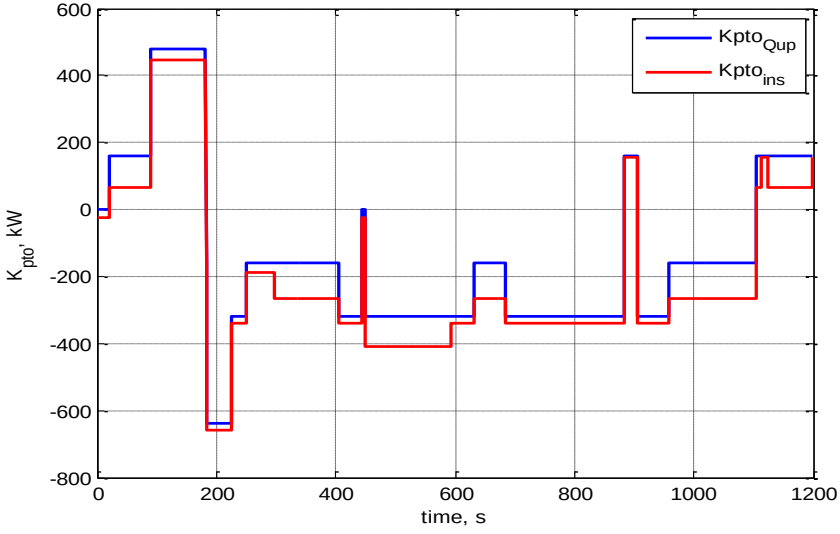

Figure 7. Quantized version of the stiffness (k_{pto}) with the instantaneously varied one.

In Figure 7, the quantized and instantaneously varied stiffness values are shown. The control approach with quantized k_{pto} is based on activating spring depending on frequency estimation. However the tuner selects upper rounding value for stiffness. From this figure it is clear that quantized levels of stiffness are technically more feasible than instantaneously varied type as variations are not instantaneous, far more practical and achievable.

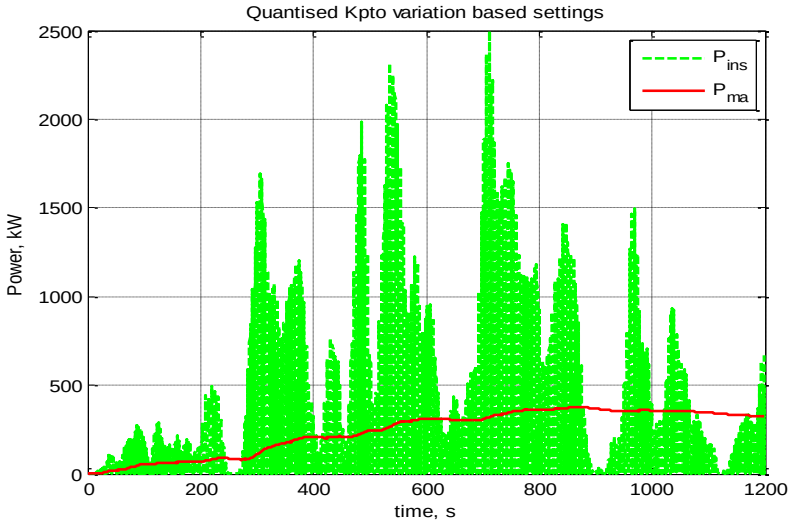

Figure 8. Power analyses for Case 2

In Figure 8, the simulation results for power analyses of Case 2 are given. In this approach, power capture is about 326kW and this corresponds to approximately 60% of the power capture of the Case 1. The main reason for loss of captured power is mismatched natural frequencies of the WEC and wave.

4.3 Case3:Quantized k_{pto} with support of FL based slow tuning control (m_{st})

Keeping the WECs at resonance by adjusting the WEC natural frequency (ω_n) to match the incident wave frequencies is the main phenomena for phase control to harvest maximum energy. In Case 2, a reasonable solution is applied to model to make WEC more realistic but resonance condition couldn't be completely satisfied. In this case (Case 3), m_{st} is determined to meet the resonance condition.. Four symmetric pumps are placed to pump water in to a tank to control added water mass (m_{st}) of WEC to meet the resonance conditions. These pumps are driven by FL controller depending on the incident wave frequencies. The FL controller rules are given in Figure 9. The simulation results of the power capture performance for Case 3 are given in Figure 10.

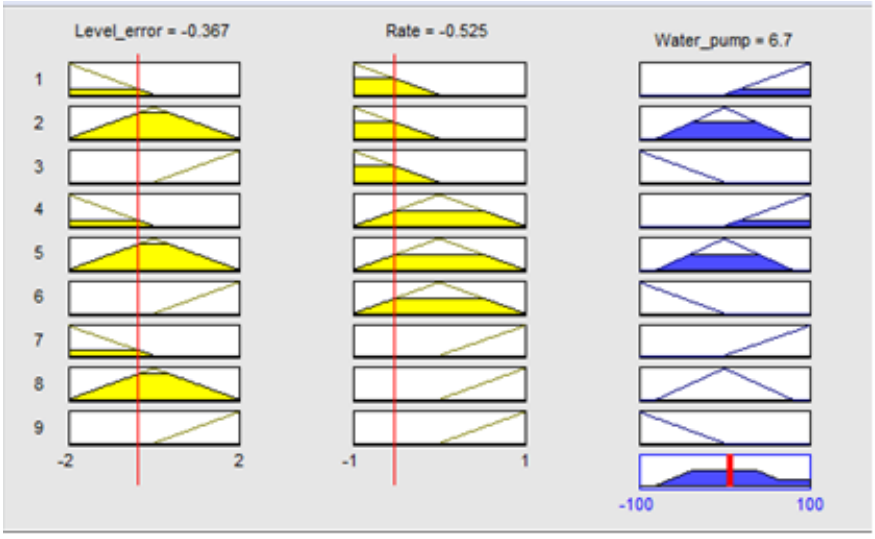

Figure 9. FL controller rules for Case 3

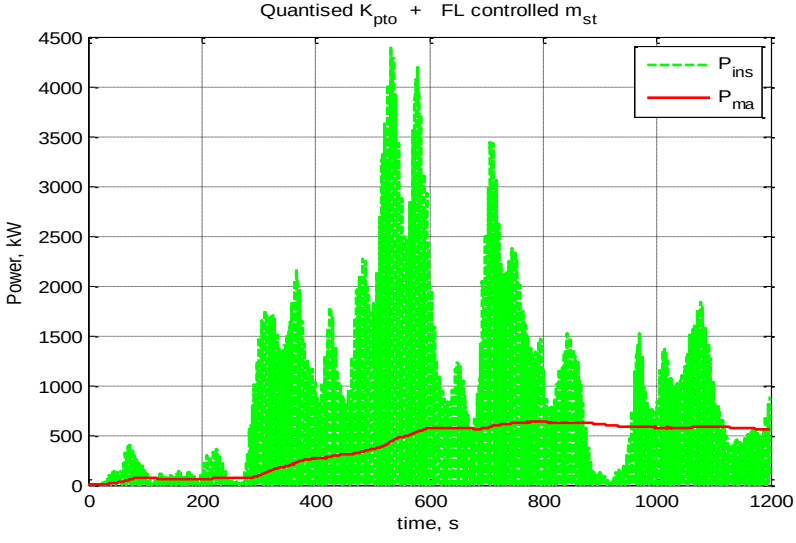

Figure 10. Power analyses for Case 3

In Figure 10, the power capture performance results are shown where quantized k_{pto} with the help of the FL controller based slow tuning appears to improve system performance very much. With the help of FL based slow tuning control approach, the deviated resonance condition met again and the total power captured by WEC is increased to 560 kW. This results indicate that less frequent variation of PTOS stiffness and slow

tuning can also be a very good and practical solution to the control problem. As this approach does not require instantaneous variation of control parameters, it leads to more practical, energy efficient and technically more feasible solution.

5 Conclusion

The objective of this paper is to determine a Fuzzy Logic controller for typical heaving wave energy converter. The proposed controller has ability to get power by achieving quantization of k_{pto} with the help of slow tuning method instead of adjusting the stiffness of PTO instantaneously. The system is modelled and simulations are done step by step to make the system more efficient and more realistic. In the first case the system has ability to capture more power but the power requirement for control approach is calculated as more higher than the power actually produced. In order to reduce the required operational energy, the quantized system is proposed as a practical solution. The power capture results for Case 2 are shown to have decreased. However, the system is practically achievable and feasible. In order to regain the energy loss due to mismatched natural frequencies, FL based slow tuning technique is proposed. The approach proposed in Case 3 appear to be more efficient and far more practical. It was clearly seen that, in order to increase the efficiency of power production, the WECs must be controlled and the resonance must be matched.

Acknowledgements

The authors would like to acknowledge the financial support of this work by the Scientific Research Projects (BAP) of the Çukurova University under the Project ID Number: 6726.

References

[1] A. Burgaç and H. Yavuz, “Control Techniques for Oscillating Wave Energy Converters,” presented at 6th International 100% Renewable Energy Conference, 2016, pp.66-74.

[2] M. Jama, A. Wahyudie, A. Assi and H. Noura, “An Intelligent Fuzzy Logic Controller for Maximum Power Capture of Point Absorbers,” *Energies* vol. 7, pp. 4033-4053, 2014.

[3] T. W. Thorpe, *“A Brief Review of Wave Energy”*, ETSU Report Number R-120 for the DTI, May 1999.

[4] H. Yavuz, T. Stallard, A. P. McCabe and G. Aggidis, "Time series analysis-based adaptive tuning techniques for a heaving wave energy converter in irregular seas," *Proceedings of the Institution of Mechanical Engineers Part A Journal of Power and Energy* , vol. 221, pp. 77-90 ,February 2007

[5] K. Freeman, M. Dai and R. Sutton, “Control strategies for oscillating water column wave energy converters,” *Underwater Technology*, vol. 32, pp. 3-13, March 2014.

[6] A. Wahyudie, M. A. Jama, A. Assi and H. Noura, “ Sliding Mode and Fuzzy Logic Control for Heaving Wave Energy Converter” presented at 62nd IEEE Conference on Decision and Control, Florance, Italy, 2013, pp. 1671-1677.

[7] C.J. Cargo, A.J. Hillis and A.R. Plummer, "Strategies for active tuning of wave energy converter hydraulic power take-off mechanisms," *Renewable Energy,* vol.94, pp. 32-47, March 2016.

[8] J. Falnes, *Ocean Waves and Oscillating systems.* Cambridge: Cambridge University Press, 2002

[9] S. Mistikoglu and H. Yavuz, "Quantized control settings based tuning of a heaving wave energy converter in irregular seas," *International Journal of Green Energy* vol 13, pp. 1281-1291, May 2016

[10] Fuzzy Logic, *Stanford Encyclopedia of Philosophy*. Bryant University. 2006-07-23. Retrieved 2008-09-30.

[11] L. A. Zadeh, "Fuzzy sets". *Information and Control*. vol.8, pp. 338–353. 1965.

[12] V.Novák, I. Perfílieva, and J. Močkoř, (1999) Mathematical principles of fuzzy logic Dodrecht: Kluwer Academic. ISBN 0-7923-8595-0

[13] M. P. Schoen, J. Hals, and T. Moan, "Wave Prediction and Robust Control of Heaving Wave Energy Devices for Irregular Waves," *IEEE Transactions On Energy Conversion,* vol. 26, pp. 627-638, June, 2011.

[14] H. Yavuz, A. P. McCabe, G. Aggidis and M. B. Widden, "Calculation of the performance of resonant wave energy converters in real seas", *Proceedings of the Institution of Mechanical Engineers, Part M. Journal of Engineering for the Maritime Environment* vol. 220(M3), pp. 117–28, March 2006

[15] MATLAB version 9a, , The MathWorks, Inc., 3 Apple Hill Drive, Natick, Massachusetts, 01760-2098, USA, 2009.

10TH INTERNATIONAL CONFERENCE ON SUSTAINABLE ENERGY AND ENVIRONMENTAL PROTECTION (JUNE 27TH – 30TH, 2017, BLED, SLOVENIA), MARINE AND HYDRO POWER
J. Krope, A.Ghani Olabi, D. Goričanec & S. Božičnik

Investigation of Spontaneous Dewatering of Sugarcane Juice Through Forward Osmosis at Module Level Employing Virgin Sea Bittern as Draw Solution

RHEA BHANSALI, BHARAT HONMANE & PUSHPITO K. GHOSH

Abstract Sea bittern is highly concentrated in inorganic salts and its osmotic pressure is more than fifteen times higher than of seawater. It has been demonstrated previously that sea bittern can be utilized as draw solution in Forward Osmosis (FO), and efficient dewatering of sugarcane juice was demonstrated. The study was carried out only at membrane coupon level. The present study extends the practical utility of the approach by reporting results at module level with ca. 100-fold scale-up of active membrane area. A hollow fibre (HF) FO module (Aquaporin make) having 0.6 m2 active area on lumen side was used for the study. An experiment was conducted in continuous single pass mode, wherein sugarcane juice (15 oBx initial density) and virgin bittern (28 °Bé density) were passed through the module at mass flow rates of 100 g min-1 and 500 g min-1, respectively. The juice collected at the outlet of the module measured 30 oBx and the dewatering performance was steady. The pure water permeate flux over 8 mins of continuous operation was computed to be 5.1 Lm-2h-1. The problem of membrane fouling was minimal and the module could be cleaned easily after use.

Keywords: • forward osmosis • sea bittern • sugarcane juice concentration • module level • single pass •

CORRESPONDENCE ADDRESS: Rhea Bhansali, Project Assistant, Institute of Chemical Technology, Chemical Engineering Department, Mumbai, Nathalal Parekh Marg, Matunga, Mumbai – 400019, India, e-mail:rheabhansali.rb@gmail.com. Bharat Honmane, Project Assistant, Institute of Chemical Technology, Chemical Engineering Department, Mumbai, Nathalal Parekh Marg, Matunga, Mumbai - 400019, India, e-mail:bharathonmane@gmail.com. Pushpito Ghosh, Ph.D., K. V. Mariwala-J. B. Joshi Distinguished Professor, Institute of Chemical Technology, Chemical Engineering Department, Mumbai, Nathalal Parekh Marg, Matunga, Mumbai - 400019, India, e-mail: pk.ghosh@ictmumbai.edu.in.

https://doi.org/10.18690/978-961-286-055-4.2 ISBN 978-961-286-055-4

Available at: http://press.um.si.

1 Introduction

The annual global production of common salt has touched 280 million tons, of which solar sea salt comprises a sizable fraction. India itself produces ca. 25 million tons of solar salt. The by-product mother liquor is referred to as sea bittern [1]. Approximately 1 m3 of pristine sea bittern of 28-29 °Bé [°Bé = 145(1-1/ρ), where ρ= specific gravity] is obtained per ton of salt produced, and it can be evaporated further to still higher densities [2],[3]. Sea bittern is highly concentrated in inorganic salts, with water activity and osmotic coefficient values in the range of 0.70-0.36 and 1.4-3.3, respectively, when the density of the bittern is in the range of 28-39 °Bé, making it an abundant reserve of pent-up energy. Much of it is discharged to sea without tapping this energy. Sugar is another high volume commodity, and India alone produces 21-24 million tons of this valuable natural product which finds wide utility in the food and beverage sector and has industrial applications also. Sucrose is used extensively, for example, in the pharmaceutical industry to make medicinal drugs more palatable [4]. It is also used to produce surfactants [5],[6] and polymers [1],[7],[8]. Sucrose is obtained primarily from sugarcane and sugar beet, Indian production being dependent exclusively on the former. For each ton of burned and cropped sugarcane delivered to the factory, ca. 600 kg of water must be stripped off to produce around 120 kg of sugar [9]. The thermal energy is largely supplied through the combustion of sugarcane bagasse, which is a resource that finds alternative uses also.

Several studies have been conducted over the years to minimize dewatering cost in sugar production. The traditional burned and cropped method of harvesting the cane no doubt would reduce the moisture content of the cane to some extent. Other methods include membrane distillation [10] and reverse osmosis [11]. Yet another emerging technique is Forward Osmosis (FO)[12-14]. It was found that sea bittern serves as efficient osmotic agent through its application as draw solution in FO [14]. Besides serving as an efficient osmotic agent, sea bittern has the additional virtues of being benign and non-toxic, making it well suited to edible applications. Indeed, dewatering of sugarcane juice was successfully demonstrated, albeit at a small scale employing a membrane coupon. The present study advances the concept through dewatering studies at module level with 100-fold higher membrane area, and employing virgin sea bittern as draw solution.

2 Material and methods

Sugarcane juice was obtained from a juice vendor and the sucrose content was estimated using a Brix meter. Sea bittern of 28.0 °Bé density was procured from a local salt works in Wadala, Mumbai. The bittern typically has the composition shown in Table 1[15].

The HF FO module used in the present study was provided by M/s Aquaporin, Denmark.

Figure 1. Solar salt works at Wadala, Mumbai from where pristine bittern of 28 °Bé density was sourced.

The specifications and other details are provided in Table 2. Feed and draw solutions were circulated using peristaltic pumps supplied by ELECTROLAB INDIA PVT. LTD. The FO experiments were performed at room temperature (28-32oC), both in recirculation mode and in continuous single pass mode. Schematic drawing of the FO assembly in recirculation mode and continuous single pass mode are shown in Figures 2 and 3, respectively.

Table 1. Typical Composition of 28 °Bé sea bittern

Parameter	Value
Specific gravity	1.24
Density on Baume scale (°Bé)	28
pH	6.8
$[Na^+]$ (M)	3.0
$[Na^+] : [K^+] : [Mg2^+] : [Ca2^+]$ molar ratio	10 : 1.1 : 5: 0.004
$[Cl^-]$ (M)	7.7
$[Cl^-]$: $[SO42^-]$ molar ratio	16:1

Table 2. Specifications of Aquaporin FO module employed in the present study

1	Test Conditions	300ml/min flow speed in lumen; 300ml/min flow speed on shell side
2	NaCl reverse flux	<2.5g/m^2/hr(0.2 oz/f^2/day)
3	Water flux	>7l/m^2/hr(4 gal/f^2/day)
4	Efficiency	<0.43g/l(0.06 oz/gal) (draw solution loss per liter of output)
5	Aquaporin Inside TM coating	Coating of Aquaporin proteins on lumen side of fiber
6	Active area	0.6m^2(6.46f^2)/1m^2(10.77f^2)
7	Number of fibers	3000
8	Rejection of fluorescent marker	>99.5% (M.W=622.55)
9	Inner diameter of fibers	(300±40)µm
10	Module dimensions	265mm long(10.43 in), 55 mm in diameter(2.17in)
11	Connectors	Ø15mm (0.59 in)
12	Process Recommendation	pre-filtration of the solution to be applied to the lumen side.
13	Shelf life	Minimum 6 months
14	Storage	Stored at room temperature, but referred storage at 4˚C(39˚F)
15	Packaging	The module is mechanically robust and is suitable for transport without additional packaging

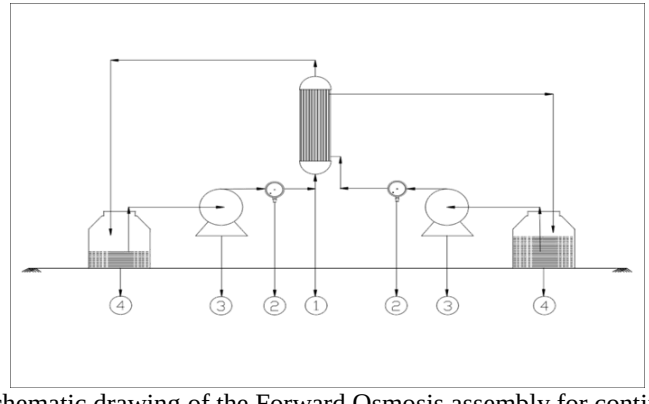

Figure 2: Schematic drawing of the Forward Osmosis assembly for continuous single pass dewatering in recirculation mode showing (1) Hollow fiber forward osmosis module, (2) pressure gauges, (3) peristaltic pumps, (4) Left: Feed Solution; Right: Draw Solution, and (5) Left: Dewatered Feed Solution, Right: Diluted Draw Solution

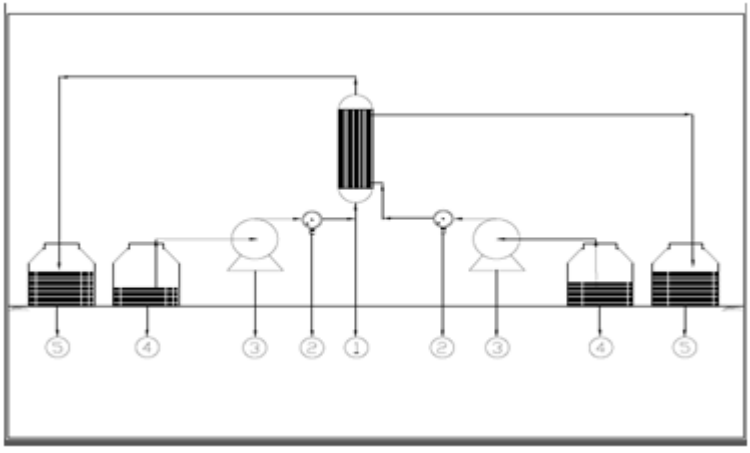

Figure. 3. (A) Schematic drawing of the Forward Osmosis assembly for continuous single pass dewatering showing (1) Hollow fiber forward osmosis module, (2) pressure gauges, (3) peristaltic pumps, (4) Feed (Left) and Draw (Right) solutions, and (5) Concentrated Feed (left) and Diluted Draw (Right).

Figure. 3 (B) Picture of the actual assembly with sugarcane juice (brown liquid) at left and bittern (pale yellow liquid) at right. Outlet feed and draw solutions were collected in the empty jars shown in the picture

3 Results and discussions

FO is a highly energy efficient process as it requires virtually no input of electrical or thermal energy. Only a small amount of electrical energy is expended in circulating the feed and draw solutions through the membrane module with the help of peristaltic pumps. The draw solution is at high chemical potential and serves as an osmotic agent, extracting water from relatively dilute feed solutions through a spontaneous process. HF membranes were introduced in the sixties and have wide utility in water treatment, desalination and

gas separation technologies [16]. The HF module is also more readily amenable to cleaning. HF FO membranes are a more recent development and are being considered for diverse applications. Novel HF FO membranes are constantly being developed [17]. Aquaporin InsideTM HF FO module is one such recent product which is as yet not commercialized and units are being provided by the company only for research and piloting purposes. In a previous study, the dewatering of sugarcane juice (osmotic coefficient φ~1.01) with concentrated bittern as draw solution was demonstrated employing a coupon cut out from polyamide flat sheet FO membrane. The improvements and scale up explored in the present study to make the process practical are listed in Table 3. Most importantly an Aquaporin InsideTM HF FO module was utilized which enabled the process to be scaled up ca. 100-fold, with steady performance. Another significant difference was that the previous study employed concentrated bittern, i.e., the virgin bittern was evaporated further to higher densities which greatly reduces the water activity and enhances the osmotic coefficient from φ =1.41 at 28°Bé to φ =3.24 at 38.9°Bé.

Table 3. List of advances made in the present work compared to the previous work [14] on bittern-based dewatering of sugarcane juice

Parameters	Previous Work	Present Work
Membrane type	Flat Sheet	Hollow Fibre
Coating	Polyamide	Aquaporin proteins coating on lumen side to improve the performance
Membrane area	0.0057 m^2	0.60 m^2 (lumen side)
Sugarcane juice	10.5% (w/v) sucrose; clarified through ultrafiltration	15.0°Bx; clarified through ultrafiltration
Bittern	38.9°Bé	28.0°Bé
Feed to Draw ratio in recirculation mode	1:8 (v/v)	2:1 (w/w)
Continuous single pass FO	Not studied	Studied

It was decided to undertake the study with virgin bittern itself since it is more readily available from a salt works and no additional effort would be required on the part of salt producers.

Table 4 provides data of a study undertaken in recirculation mode (Figure 2) employing Aquaporin InsideTM HF FO module. The study was carried out with an initial 2:1 (w/w) ratio of feed (sugarcane juice) to draw (sea bittern). Thus, 1000.4 g (930 mL, ρ = 1075.3 kgm-3) of 15oBx sugarcane juice was taken in one container and 500.9 g (410 mL, ρ = 1219.5 kgm-3) of 28°Bé sea bittern in another container. The feed and was circulated through the lumen side at 100 mLmin-1 (19 rpm pump speed) and the draw was circulated at the flow rate of 100 mLmin-1 (18 rpm pump speed) through the shell side of the module. The experiment was conducted over 40 min and the change in weight of the draw solution with time is plotted in Figure 4. As can be seen from the figure, the diluted draw solution weighed 1104.5 g after 40 min, its volume was 1022 mL and its density was computed to be 1083.8 kgm-3. The weight of the feed (sugarcane juice), on the other hand, reduced to 363.7 g, its density measured 1200.4 kgm-3 and the Brix reading was 47oBx as compared to the initial reading of 15oBx. The average permeate water flux was estimated to be 1.59 Lm-2h-1. The mass balance was satisfactory (weight gain of 603.1 g of draw solution versus weigh loss of 636.7 g), the small difference being on account of hold up of solution in the module and tubing.

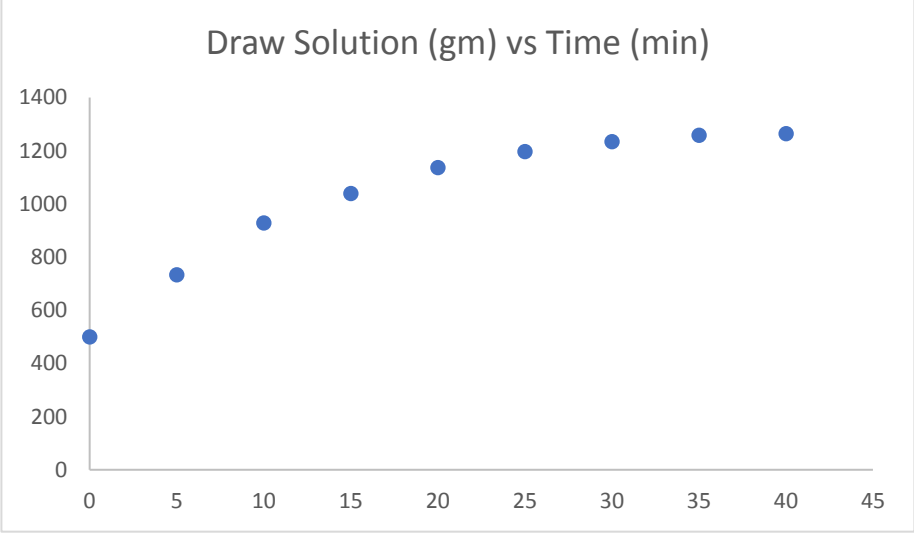

Figure 4. Plot of increase in weight of sea bittern (draw solution) versus time for experiment conducted in recirculation mode.

A second experiment was conducted in continuous single pass mode (see Figure 3). Sugarcane juice from the same lot was passed through the module at flow rate of 100 $gmin^{-1}$ (19 rpm pump speed) while the sea bittern was circulated through the shell side at 500 $gmin^{-1}$ flow rate (75 rpm pump speed). The results are plotted in Figure 5. As can be seen the cumulative volume of the draw solution increased linearly with time over the duration of the experiment (8 mins). Against the 8x100 g = 800 g (sugar content in the

total feed weight would be (15/100) x 800 = 120 g) of feed solution passed through the module in 8 minutes, the weight of concentrated feed obtained was 386.2 g. Against the estimated Brix concentration of 31 ^{o}Bx [(120/386.2)x 100], the experimentally determined value was 30 ^{o}Bx which was in good agreement. Thus the sugar concentration was doubled in the continuous single pass experiment. Considering further that the water amount that permeated from the feed solution to the draw solution was 800-386.2 g = 413.8 g over 8 mins, the average permeate water flux was computed to be (0.4138 x 60)/(8 x 0.6) $Lm^{-2}h^{-1}$ = 5.17 $Lm^{-2}h^{-1}$.

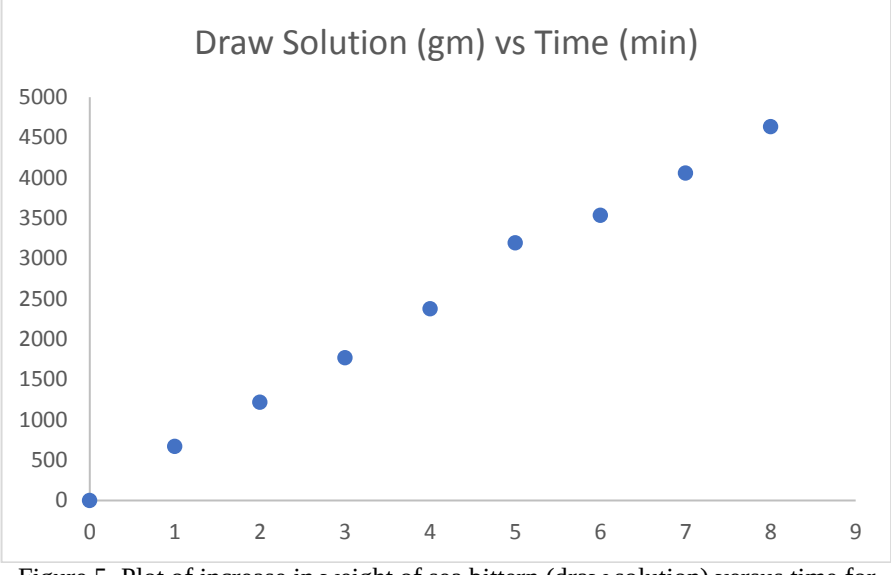

Figure 5. Plot of increase in weight of sea bittern (draw solution) versus time for experiment conducted in continuous single pass mode.

4 Conclusion

The present study investigated the practical utility of FO for dewatering of sugarcane juice with virgin bittern as osmotic agent. Doubling of the Brix concentration and a high permeate water flux (5.17 $Lm^{-2}h^{-1}$) were achieved in practical manner, i.e., through continuous single pass FO. Even with the small module employed, it would be feasible to process 140 kg of sugarcane juice over 24 h period based on the results achieved, considering 5:1 (w/w) ratio of virgin sea bittern to sugarcane juice, and a target of twofold increase in sugar concentration. The process was undertaken at room temperature. Leakage of sugar and problems due to fouling were minimal.

Acknowledgements

The authors wish to thank TEQIP Innovation Networking Project for generously supporting the work and Dr. Jyotsna Waghmare for providing the space to set up the FO unit. The authors also wish to thank M/s Aquaporin for providing an FO module for research and scale up purposes. The authors also wish to thank Mr. Rahul Pathak and Mr. V. Karunakaram for facilitating the procurement of FO module and for their keen interest in the work.

References

[1] Salt Industry in India, saltcomindia.gov.in
[2] "Bittern – Chemistry", Encylopedia Britannica.
[3] The Salt Recovery Process, New Zealand Institute of Chemistry (nzic.org.nz)
[4] Hopkins, H.; Small, L. V. D. "An investigation of some pharmaceutical applications of certain fatty acid esters of sucrose", J. Pharmaceutical. Sci., 1960, 49, 220-224.
[5] Bazin, H. G.; Polat, T.; Linhardt, R. J. "Synthesis of sucrose-based surfactants through regioselective sulfonation of acylsucrose and the nucleophilic opening of a sucrose cyclic sulfate", Carbohydrate Research, 1998, 309, 189-205.
[6] Sanders, H. L. "Sucrose-based surfactants as aids in sugar refining and sugar crystallization processes", US Patent 3476598 (1969).
[7] Jhurry, D.; Deffieux, A. "Sucrose-based polymers: Polyurethanes with sucrose in the main chain", European Polymer Journal, 1997, 33, 1577-1582.
[8] Poschalko, A. et al. "SUBPOL: a novel sucrose-based polymer support for solid-phase peptide synthesis and affinity chromatography applications." Journal of the American Chemical Society 125.44 (2003): 13415-13426.
[9] Clarke, M. A., ed. Chemistry and Processing of Sugarbeet and Sugarcane, Elsevier Science Publishing Co. Inc., 1988.
[10] Nene S.; Kaur S.; Sumod K.; Joshi B.; Raghavarao K. S. M. S., Desalination, 2002, 147, 157–160.
[11] Gul S.; Harasek M., Energy Savings in Sugar Manufacturing with the Implementation of a new Membrane Process, http://www.nt.ntnu.no/users/skoge/prost/proceedings/pres2011-andicheap10/PRES11/231Gul.pdf, 2009.
[12] der Bruggen, B. V.; Luis, P., Rev. Chem. Eng., 2014, DOI:10.1515/revce-2014-0033.
[13] Castello M. E. G.; McCutcheon J. R.; Elimelech, M., J. Membr. Sci., 2009, 338, 61–66.
[14] Mondal, D.; Nataraj, S. K.; Reddy, A. V. R.; Ghara, K. K.; Maiti, P.; Upadhyay, S. C.; Ghosh, P. K. "Four-fold concentration of sucrose in sugarcane juice through energy efficient forward osmosis using sea bittern having high osmotic coefficient as draw solution", RSC Adv., 2015, 5, 17872.
[15] Ghara, K. K.; Korat, N.; Bhalodiya, D.; Solanki, J.; Maiti, P.; Ghosh, P. K. "Mitigating Environmental Uncertainties in Conventional Potash Production from Sea Bittern: Demonstration of a Viable Scheme for Selective Extraction with Tartaric Acid", RSC Adv., 2014, 4, 34706.
[16] Feng, C. Y.; Khulbe, K. C.; Matsumara, T.; Ismail, A. F. "Recent progresses in polymeric hollow fiber membrane preparation, characterization and applications", Separation and Purification Technology, 2013, 111, 43-71.
[17] Wang, R.; Shi, L.; Tang, C.; Chou, S.; Qiu, C. et al., "Characterization of novel forward osmosis hollow fiber membranes, J. Membr. Sci., 2010, 355, 158-167.

10TH INTERNATIONAL CONFERENCE ON SUSTAINABLE ENERGY AND ENVIRONMENTAL PROTECTION (JUNE 27TH – 30TH, 2017, BLED, SLOVENIA), MARINE AND HYDRO POWER
J. Krope, A.Ghani Olabi, D. Goričanec & S. Božičnik

Zuppinger Water Wheel for Very Low-Head Hydropower Application

SHAKUN PAUDEL, MARTIN WEBER, DIRK GEYER & NICOLE SAENGER

Abstract Very low-head hydropower sites are abundantly available on small rivers, streams, irrigation canals, headworks or at wastewater facilities. However, lack of economically and ecologically viable technologies has been impeding these sites from being utilised for hydropower. The Zuppinger water wheel, with its high efficiencies over a wide operating range, is a potential device for very low-head applications. The efficiencies of around 75 % quoted in the literature reflect that there still exists a potential to improve the wheel performance through a better understanding of the flow physics around the wheel. For this reason, a test-rig with a Zuppinger water wheel model and a non-intrusive velocity measurement technique, Particle Image Velocimetry (PIV) is developed. In this paper, the experimental set-up, PIV instrumentation, and the special requirements on the set-up imposed by the water wheel are discussed and preliminary results are presented.

Keywords: • PIV • hydropower • very low-head • Zuppinger • water wheel •

CORRESPONDENCE ADDRESS: Shakun Paudel, PhD, Post-doctoral Fellow, Darmstadt University of Applied Sciences, Department of Civil Engineering, Haardtring 100, 64295 Darmstadt, Germany, email: sagunpaudel@gmail.com. Martin Weber, MEng, Research Fellow, Darmstadt University of Applied Sciences, Department of Civil Engineering, Haardtring 100, 64295 Darmstadt, Germany, email: matrin.weber@h-da.de. Dirk Geyer, PhD, Professor, Darmstadt University of Applied Sciences, Department of Mechanical Engineering, Haardtring 100, 64295 Darmstadt, Germany, email: dirk.geyer@h-da.de. Nicole Saenger, PhD, Professor, Darmstadt University of Applied Sciences Department of Civil Engineering, Haardtring 100, 64295 Darmstadt, Germany, email: nicole.saenger@h-da.de.

https://doi.org/10.18690/978-961-286-055-4.3 ISBN 978-961-286-055-4

Available at: http://press.um.si.

1 Introduction

The increasing pressure of reducing global warming has generated enormous research and development efforts in the renewable energy sector. Among which hydropower is the key player generating 71 % of total renewable energy at the end of 2015 [1]. And, there is still a considerable potential for developing hydropower resources globally.

On that context, very low-head hydropower sites of those below 5 m head differences could be an interesting source of energy. Such sites are abundantly available within irrigation systems, headworks, weirs, wastewater facilities, and at old mill sites [2]. Utilising these small but important sources of energy has until now been retarded by the lack of economically justified technological solutions.

Conventional water wheels have been used for power generation since centuries. The Zuppinger water wheel is one of the most efficient devices developed in the1850s [3]. In Europe, this wheel is widely used even today for running old mills or even for electrical power production. High efficiencies of around 75 % and power generation of more than 40 kW were quoted in the literature [4] that could be significant amount of power for decentralised application to meet the daily energy requirement.

Nonetheless, the efficiencies reported in the literature means that there is still a room to optimise the wheel for better efficiency. To understand the losses within the wheel and with an ultimate objective to optimise the wheel geometry, a test rig with a model of Zuppinger water wheel with advanced velocity measurement technique 'Particle Image Velocimetry (PIV)' is developed. PIV is a non-intrusive, highly accurate and powerful method of velocity measurement [5]. In this paper, the test-rig and PIV set-up is described in detail. The challenges imposed by the air entrainment and the complexity of the structural components on the PIV set-up are discussed, and some preliminary results on the wheel performance are presented.

2 The test-rig

The test-rig consists of a purpose built 17.3 m long, 0.8 m wide, and 0.7 m high flume with a model Zuppinger wheel and PIV measurement facility. The wheel has a 1.2 m diameter and is 79.2 cm wide with a maximum of 24 blades. The blades are made up of 8 mm thick PMMA sheet. The wheel is placed over a curved shroud made up of 12 mm thick float glass to allow the laser sheet to intersect from underneath the flume. A gap of 4 mm is kept between the sides and bottom of the flume and the wheel.

The flow in the flume is measured using Krohne Optiflux 2100 series electromagnetic flow meter with an accuracy of ± 0.3 %. A magnetic powder brake FRAT 350 from Liedtke with torque transducer TRS 50 (accuracy ± 0.5 % of full scale at 20°C) was used for measuring the torque on the wheel shaft. The rotational speed of the wheel is measured with solid shaft encoder from IFM model RB1015. Downstream submergence of the wheel has a significant impact on the wheel performance. To reproduce the

downstream water levels accurately, an inclination sensor INY360D-F99-2U2E2-V17 from Pepperl+Fuchs (accuracy ± 0.5°) is used for positioning of the downstream weir.

The optical set-up uses dual oscillator pulsed Nd:YAG laser (Spitlight compact DPSS 100) having a 532 nm wavelength, minimum 50 mJ pulse energy, pulse frequency of 100 Hz and pulse duration of 7–9 ns. It also contains an integrated cooling unit. To guide the 5 mm diameter laser beam into the flume, a Periscope with 1" mirror, two 2" mirrors, a concave lens (f = -40 mm) and two convex lenses (f = 300 mm and f = 1000 mm) and a 3", 90° mirror were used. The laser beam is thus converted into a ≈110 mm wide and ≈1 mm thick laser sheet for 2D PIV measurement. Figure 1 shows the PIV instrumentation.

A Programmable Timing Unit (PTU) from LaVision (model PTU9) is used for the synchronisation of the camera, lasers and the wheel and to readout the synchronised data from all sources. A rotary decoder is integrated into the PTU for precise phase triggering. A LaVision Imager sCMOS camera (2560 x 2160 px) with a 532 nm interference filter and a 200 mm AF Micro-Nikkor 1:4D IF-ED objective was used for imaging. The maximum frame rate of the camera is 50 Hz.

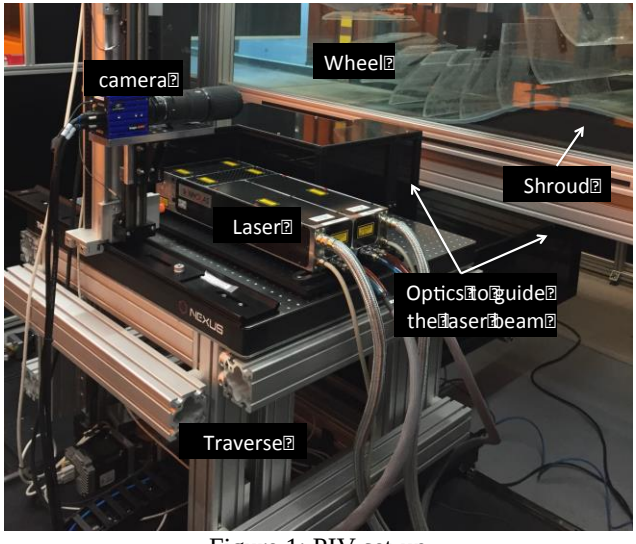

Figure 1: PIV set-up

2D PIV software module, with processing software DaVis 8.2 is used. The size of a Field of view (FOV) is approximately 95 x 80 mm, so multiple frames are required to capture the flow field around the wheel blades. A calibration target was developed to serve the purpose of measurement calibration. The breadboard with laser, camera and the optical parts are carried by an in-house developed 3D traverse system. The traverse can be moved in all coordinate direction with a repeatability of 0.05 mm. The camera can be moved in the z-axis independent of the traverse.

The head difference, power output and efficiency of the wheel are calculated using Eq. (1–3). Where, h is water depth in m, v is velocity in m/s. The subscripts 1 and 2 refer to the upstream and downstream of the wheel, respectively. The velocity is calculated from the known flow rate (Q) and the wetted flow area ($v_1=Q/Bh_1$; $v_2=Q/Bh_2$). The geodetic head difference between the upstream and downstream of the wheel (z_1-z_2) is 9.3 cm; ω (=2πN/60) is the angular velocity of the wheel in rad/s and N is the rotational speed in rpm.

$$H = \left[z_1 + h_1 + \frac{v_1^2}{2g} \right] - \left[z_2 + h_2 + \frac{v_2^2}{2g} \right] \quad \text{Eq. (1)}$$

$$P_{out} = wt \quad \text{Eq. (2)}$$

$$h = \frac{wt}{rgQH} \times 100\% \quad \text{Eq (3)}$$

A cRIO-9074 was used to acquire data. A LabVIEW environment is programmed to control input parameter and real time monitoring of the data.

3 Seeding particles

Correct choice of seeding particles is very important in successfully conducting PIV measurements. Seeding particles should possess physical properties that allow them to accurately follow the flow pathlines and match with the flow acceleration, as well as the particles must have adequate scattering characteristics [6]. The diameter and density of the particles are the deciding factors in describing the ability of the particle to follow the flow and their scattering characteristics. As such, particles must be small enough to follow the flow pathlines and at the same time large enough for yielding high signal-to-noise ratio (SNR) of the scattered light signal [6, 7]. Moreover, the concentration of the particle is equally important.

However, while choosing a diameter a compromise must be made between the tracking capability and scattering characteristics of the particles. After a discussion with different manufacturers, particles of diameter around 1-10 μm were recommended as suitable for the current application. Besides the particle diameter, Mei [8, p6] recommends the ratio of particle density to the fluid density from 0.56 to 1.62 for very good response of seeding particles. In this case, considering water density of 0.9982 g/cm^3 at 20°C and mean particle density of 1.1 g/cm^3, specific gravity resulted in a value of 1.101.

Particle concentration of 8–10 particles per interrogation area (IA) is suggested in the literature [9]. To determine the right concentration of the particles for the current application, number of particles present in the IA (32 x 32 px) was visually evaluated in

DaVis. For the desirable concentration of particles (8–10 particles per IA), 2.25 g of particles is required per 100 l water. The total volume of 20 m^3 water in the flume thus requires 450 g particles for one time seeding.

Following the general guidelines for particles that they are non-toxic, non-corrosive, non-abrasive, non-volatile and chemically inert [6], different particles within the preferred diameter and density range were considered in the preliminary analysis. These particles include polyamide, Hollow Glass Sphere (HGS) particles from three different manufacturers and fluorescent polymer particles. However, due to the high costs for the fluorescent polymer particles (further described in Section 4), only polyamide seeding particles from Dantec and HGS particles from three different manufacturers (LaVision, Dantec and TSI) were tested for their suitability in the current application. Considering different criteria such as agglomeration, mixing, floating, sinking with time and cost, HGS particles from TSI were found suitable for this application. These particles have a mean diameter of 10 μm, a density of 1.1 g/cm^3, and refractive index of 1.52.

4 Multiphase flow

The flow in the flume is turbulent with Reynolds number ranging from 18000 to 42000. Due to the interaction of wheel blade at the free surface, the turbulence at the free surface becomes large enough to overcome the effect of surface tension and gravity forces. Then, air entrainment in the water becomes evident. The flow becomes multiphase containing different size of air bubbles. This entrained air bubbles alter the turbulent energy of the flow [10]. Thus, in such flows it is essential to capture the flow velocities in both phases.

Unlike single-phase flow, a number of technical problems arise in applying PIV in multiphase flow [11]. The air bubbles entrained into water also reflect on the laser light. The reflected light from air bubbles is not homogenous and reflection depends on the angle of incidence [12, p204]. In such flows, the velocity obtained through the conventional correlation method is an average velocity calculated based on the signals from both tracer particles in water phase and air bubbles in air phase. If the difference in velocities between these two phases is large, then it produces unrealistic velocity values [11]. The limitations of PIV on multiphase flow measurement are discussed by [13].

A handful of literature is dedicated to the PIV techniques in multiphase flows. One of the widely used approaches for multiphase flow is the use of fluorescent particles as seeding particles (eg. [14]–[18]). This method requires high pass optical filter to separate the radiation scattered by fluorescent and neutral particles [19]. A high-speed camera records the laser induced fluorescence (LIF) signal of the seeding particles and a second camera records the light reflected from air bubbles. However, the air bubbles also reflect the LIF signal of the seeding particles and can generate an erroneous measurement signal in the liquid flow. The measurement of the velocity of air bubbles is also influenced by the curvature effect [20].

An alternative approach employs a digital masking method to separate the signals coming from different phases as discussed by [21] and [22]. If the illumination of air bubbles is uniform, the digital masking can be applied based on the particle size. If this is not the case, digital mask can be generated using advanced image processing techniques [20].

Another commonly used technique is the combination of 2D PIV for liquid phase, 3D particle tracking velocimetry (PTV) for air (bubbles) and shadowgraphy. Furthermore, Lindken and Merzkirch [20] present a novel method combining the PIV with fluorescent particles, digital masking technique and shadowgraphy. Today, multiphase flow measurement techniques are well established and are available in commercial packages with fluorescent particles and shadow-imaging cameras to meet customised requirements. For example, DaVis uses PIV with fluorescent particles for continuous (liquid) phase and time-resolved shadowgraphy for air bubbles size, shape and velocity.

In the current state of the test-rig, flow being seeded with HSG particles and with entrained air, vectors are incorrectly captured as expected. As shown in Figure 2, wrong vectors are built up on the surface of blade due to reflection and air entrainment.

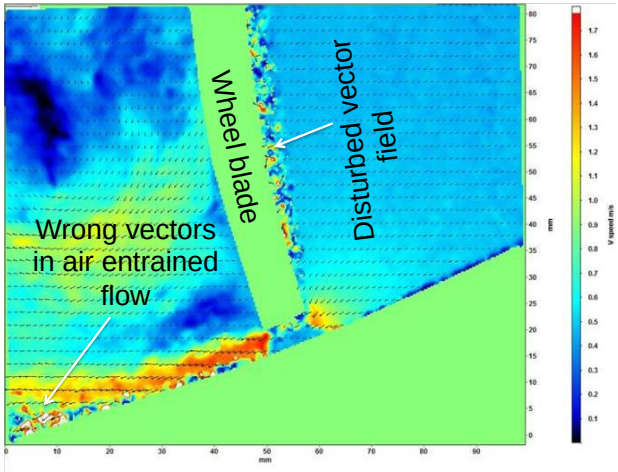

Figure 2: Vectors around the wheel blade

To address the air bubbles entrainment and light reflection (discussed in Section 5), use of fluorescent particles and shadowgraphy will be an option. However, the use of commercial fluorescent particles implies unreasonably high costs of about €35,000 for one time seeding, i.e. 240 times higher costs compared to HSG. An alternative option would be to produce fluorescent particles as done by other researchers (eg. [18]).

5 Curved and reflective surfaces

The test-rig consists of curved structural elements and reflective surfaces having different refractive index. The camera sensor signals pass through different mediums, i.e. air to solid (glass), to liquid (water). The glass, water, and air have refractive index of 1.52, 1.33 and 1.00, respectively. Due to this, errors are generated in the image magnification. Calibration of the test set-up is therefore necessary to negate the distortion, perspective-errors and to minimise the error in calculating the magnification factor. A calibration target is developed in-house for that purpose.

Moreover, the blade surface produced strong reflection of the laser light as seen in Figure 3. This reflection can decrease the SNR value and also affect the camera [23].

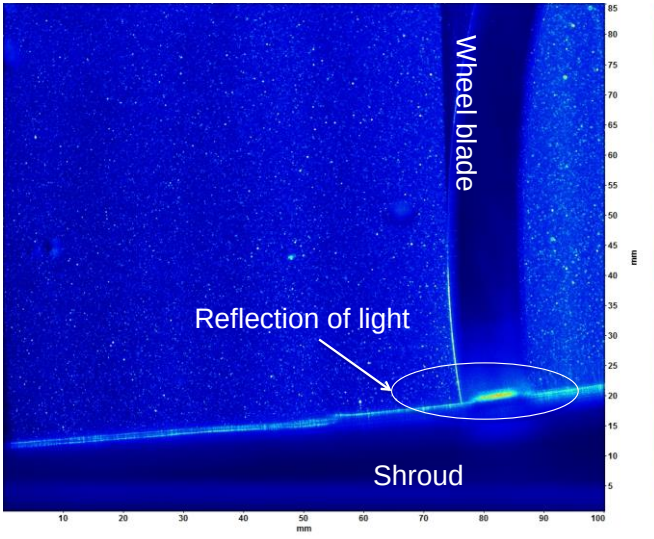

Figure 3: Reflection of light on the surface

6 Wheel performance

The model tests have shown maximum efficiency of the wheel up to 88 %. This efficiency is even higher than the values reported in the literature. Wheel efficiency as a function of tangential velocity of the wheel ($v=\omega r$) at different flow rates and downstream submergence level is plotted in Figure 4. The grey and black lines represent the downstream water level (h_2) of 15 cm and 20 cm, respectively.

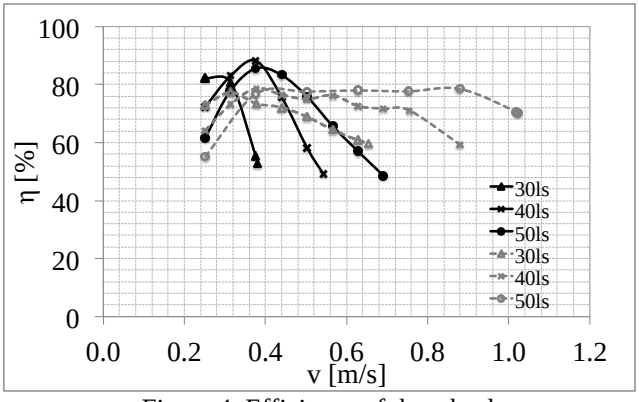

Figure 4: Efficiency of the wheel

At 15 cm downstream water level, efficiency curves are much flatter and wider. However, as the submergence level increases (h_2=20 cm), the efficiency drops rapidly at higher velocity showing a narrower band for wheel operation.

Power output of the wheel at different flow rates and downstream water levels is plotted in Figure 5. At 50 l/s flow rate, power output reached about 70 W. At the lower downstream submergence level (h_2=15 cm) and at higher velocity of the wheel, power output remains almost constant. These results show the possibility of constant power generation at wide operating range of the wheel. The maximum uncertainties in the measurement of efficiency and power output are 2.5 % and 2 W, respectively.

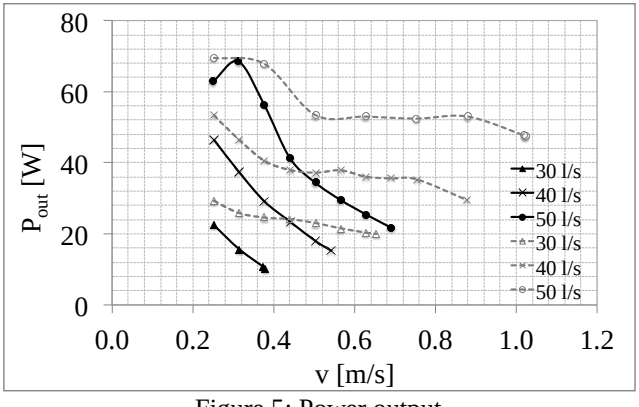

Figure 5: Power output

7 Conclusion

Even though larger part of the hydropower potential is already harnessed in industrialised countries, there are still areas to generate handful amount of hydropower from very low-

head sites. Zuppinger water wheel is a suitable device for such applications. Their high efficiency, simplicity in design and slow rotational speed offers an economically and environmentally sustainable solution.

PIV is a powerful method to study the fluid flow. Application of PIV in the special case described in this paper is novel to the best of authors' knowledge. As discussed above, the test-rig in its current state has multiple technical challenges, which are currently being addressed for acquiring high quality phase-resolved PIV measurements on the Zuppinger water wheel model.

Acknowledgements

This research is funded by the German Ministry of Education and Research (BMBF) under grant number 03fH021I2.

References

[1] World Energy Council, "World energy resources | 2016" World Energy Council, ISBN: 978 0 946121 62 5, London, 2016.
[2] S. Paudel "Experimental and numerical study of Dethridge wheel for pico-scale hydropower generation, *PhD Thesis*, Darmstadt University of Technology, 2016.
[3] D. M. Nuernbergk, *Wasserräder mit Kropfgerinne: Berechnungsgrundlagen und neue Erkenntnisse*. [In German] Detmold: Schäfer, 1st edition, 2005.
[4] G. Müller, G. and C. Wolter, "The breastshot water wheel: Design and model tests" In Proceedings of the institutions of the civil engineers: Engineering Sustainability, 2004.
[5] R. J. Adrian, "Particle imaging techniques for experimental fluid mechanics", *Ann. Rev. Fluid Mech*., vol. 23, pp. 261–304, 1991.
[6] A. Melling, "Tracer particles and seeding for particle image velocimetry", *Measurement Science and Technology*, vol. 8, pp. 1406–1416, 1997.
[7] Y. A. Hassan, W. D. Schmidl and J. Ortiz-Villafuerte, "Three dimensional bubbly flow measurement using PIV", *Journal of Visualisation*, vol. 1, No. 3, pp. 291–301, 1999.
[8] R. Mei, "Velocity fidelity of flow tracer particles", *Experiments in Fluids*, vol. 22, pp. 1–13, 1996.
[9] L. Lu and V. Sick, "High-speed particle image velocimetry near surfaces", *Journal of Visualized Experiments : JoVE*, vol. 76, 2013.
[10] T. G. Theofanous and J. Sullivan, "Turbulence in two-phase dispersed flows" *Journal of Fluid Mechanics*, vol. 116, pp. 343–362, 1982.
[11] W. Merzkirch, L. Gui, S. Hilgers, R. Lindken and T. Wagner, "PIV in multiphase flow" Proceedings of the second international workshop on PIV, Fukui, 1997, pp. 165–171.
[12] R. Lindken, L. Gui and W. Mezkirch, "Velocity measurement in multiphase flow by means of particle image velocimetry", *Chemical Engineering Technology*, vol. 22, pp. 202–206, 1999.
[13] C. Brücker, "PIV in two phase flows", *Lecture Series 2000-01, Particle Image Velocimetry and associated techniques*, Jan. 17-21, Von Karman Institute for Fluid Dynamics, ed. by M.L. Riethmuller, Rhode-St-Genese, Belgium, 2000.
[14] T. C. Fu, R. Bing, J. Katz and T. T. Huang, "Automatic particle-image velocimetry utilizing laser-induced fluorescent particles," The proceedings: Fifth international conference on

numerical ship hydrodynamics, Washington D.C.: The National Academies Press, 1990, pp. 493-498.

[15] Y. A. Hassan, and O.G., Philip and W. G. Schmidl, "Bubble collapse velocity measurements using a particle image velocimetry technique with fluorescent tracers", *ASME Fluid Element Dynamics,* vol. 172, pp. 85–92, 1993.

[16] G. Sridhar and J. Katz, "Drag and lift forces on microscopic bubbles entrained by a vortex", *Physics of Fluids*, vol. 7, No. 2, pp. 389–99, 1995.

[17] D. P. Towers, C. E. Towers, C. H. Buckberry and M. Reeves, "A colour PIV system employing fluorescent particles for two-phase flow measurements", *Measurement Science and Technology*, vol. 10, pp. 824–830, 1999.

[18] D. E. Turney, A. Anderer and S. Banerjee, "A method for three-dimensional interfacial particle image velocimetry (3D-IPIV) on an air-water interface", *Measurement Science and Technology*, vol. 20, pp. 1–12, 2009.

[19] Y. A. Hassan, W. D. Schmidl and J. Ortiz-Villafuerte, "Investigation of three-dimensional two-phase flow structure in a bubbly pipe flow", *Measurement Science and Technology*, vol. 9, pp. 309–326, 1998.

[20] R. Lindken and W. Mezkirch, "A novel PIV technique for measurements in multiphase flows and its application to two-phase bubbly flows ", *Experiments in Fluids*, vol. 33, pp. 814–825, 2002.

[21] L. C. Gui and W. Merzkirch, "A method of tracking ensembles of particle images" *Experiments in Fluids*, vol. 21, pp. 465–468, 1996.

[22] L. Gui, S. T. Wereley and Y. H. Kim, "Advances and applications of the digital mask technique in particle image velocimetry experiments", *Measurement Science and Technology,* vol. 14, pp. 1820–1828, 2003.

[23] B. J. Petrosky, P. Maisto, K. T. Lowe, M. A. André , P. M. Bardet, P. I. Tiemsin, C. J. Wohl and P. M. Danehy, "Particle image velocimetry applications using fluorescent dye-doped particles", 53rd AIAA Aerospace Sciences Meeting, 2015.

10TH INTERNATIONAL CONFERENCE ON SUSTAINABLE ENERGY AND ENVIRONMENTAL PROTECTION (JUNE 27TH – 30TH, 2017, BLED, SLOVENIA), MARINE AND HYDRO POWER
J. Krope, A.Ghani Olabi, D. Goričanec & S. Božičnik

Can Full-Scale Pressure Retarded Osmosis System Derive Energy from the Ocean?

MINSOO KIM & SUHAN KIM

Abstract Pressure retarded osmosis (PRO) produces energy using the salinity gradient between two solutions (draw solution (DS) and feed solution (FS)). Using one of the best PRO membranes available so far, the ideal power production from seawater could be up to 4 watts per unit membrane area (m2) under a realistic hydraulic condition. In this work, a full-scale PRO model was developed to estimate the net energy production using the salinity gradient between seawater and fresh water. The model accounts for the fundamental mass transfer in PRO (e.g., internal and external concentration polarization), the scale-up effect (e.g., diluted DS and concentrated FS) and the efficiencies of hydraulic devices. The net energy was estimated using the model simulation, which revealed that a full-scale PRO can derive energy from seawater up to 36.8 Wh/m3. However, if the energy for pretreating DS and FS is considered, the net energy becomes negative.

Keywords: • pressure retarded osmosis • full-scale model • seawater • net energy • hydraulic devices •

CORRESPONDENCE ADDRESS: Minsoo Kim, Pukyong National University, Department of Civil Engineering, 45 Yongso-ro, Nam-gu, Busan, 48513, Korea; email: minseok9928@gmail.com. Suhan Kim, Pukyong National University, Department of Civil Engineering, 45 Yongso-ro, Nam-gu, Busan, 48513, Korea; email: suhankim@pknu.ac.kr.

https://doi.org/10.18690/978-961-286-055-4.4 ISBN 978-961-286-055-4

Available at: http://press.um.si.

1 Introduction

The osmotic energy of seawater is equivalent to a waterfall of 270 m. This potential can be converted into an energy form by pressure retarded osmosis (PRO) process. PRO produces osmotic energy from the salinity difference between two solutions. In a PRO process, a draw solution (DS) with high concentration draws water across a membrane from a feed solution (FS) with low concentration. The diluted and volume-expanded DS with a mechanical pressure lower than the osmotic pressure difference between DS and FS, flows through a hydro-turbine for the energy production [1].

Most PRO studies have focused on lab-scale performances of coupon-sized PRO membranes to understand the factors affecting power density such as the active and support layer characteristics, hydrodynamic conditions, and fouling [2-5]. However, power density obtained from a lab-scale membrane experiment cannot be directly converted to the energy production rate of a full-scale PRO plant due to scale-up effects such as the diluted DS and the concentrated FS inside the membrane module, inefficient hydraulic devices (e.g., pump, motor, energy recovery device (ERD), turbine, and generator), and pressure loss along the channels (e.g., the DS and FS channels, and pipelines). Thus, a net energy production (NEP) analysis based on full-scale performance should be carried out to estimate a realistic energy production potential of a PRO process.

In our work, the NEP analysis based on a newly developed full-scale PRO model was carried out. The model accounts for not only the fundamental mass transfer in PRO such as internal and external concentration polarization (ICP and ECP), but also the scale-up effects such as the diluted DS, the concentrated FS, the efficiencies of hydraulic devices as a function of the plant capacity (e.g., the sum of the FS and DS flow rates), and the hydraulic pressure drops along the membrane channels.

2 METHODS

2.1 ICP and ECP

The water flux in PRO is obtained by the osmotic pressure difference between DS and FS, and thus it is strongly affected by concentration polarization [6, 7]. As shown in Figure 1, c_1 and c_5 are the salt concentrations of the FS and DS, respectively; c_2 and c_4 are the salt concentrations at the FS–support layer and the DS–active layer interfaces, respectively; and c_3 is the salt concentration at the interface between the active and support layers. ECP causes c_2 and c_4, which are smaller than c_1 and c_4, respectively, while ICP causes c_3, which is smaller than c_2.

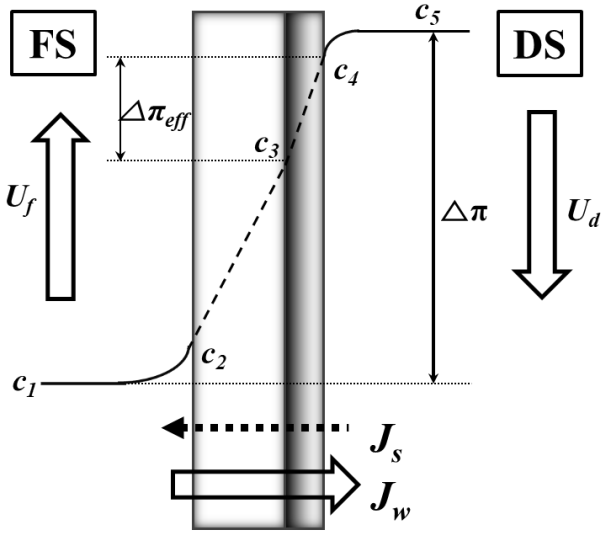

Figure 1. Concentration profile across PRO membrane

The water flux can be expressed as Equation (1).

$$J_w = A(\Delta\pi_{eff} - \Delta P) = A(\pi_4 - \pi_3 - \Delta P) \quad (1)$$

Where, J_w is water flux, A is the water permeability coefficient of the membrane, $\Delta\pi_{eff}$ is the effective osmotic pressure differential, ΔP is the hydraulic pressure differential, and π_i is the osmotic pressure driven by the concentration, c_i. The following procedure to obtaine the water flux using ICP and ECP theory is well described in our previous work [6].

2.2 Scale-up of the PRO model

A full-scale membrane process model generally accounts for changes in the operation parameters (e.g., flow rates, pressures, and concentrations) along the channel inside the membrane module [8-11]. Instead of calculating all the parameters as functions of longitudinal position, the length-averaged parameters are estimated based on mass balance in a full-scale PRO system (Figure 2) for simplicity in this work.

Water and solute mass balances on the DS and FS sides are described as:

$$Q_d + J_w A_m = Q_{dd} \quad (2)$$

$$C_{\mathrm{d}}Q_{\mathrm{d}} - J_{\mathrm{s}}A_{\mathrm{m}} = C_{dd}Q_{\mathrm{dd}} \tag{3}$$

$$Q_{\mathrm{c}} + J_{\mathrm{w}}A_{\mathrm{m}} = Q_{\mathrm{f}} \tag{4}$$

$$C_{\mathrm{c}}Q_{\mathrm{f}} - J_{\mathrm{s}}A_{\mathrm{m}} = C_{c}Q_{\mathrm{c}} \tag{5}$$

Where, Q, C, J, and A_m are flow rate, salt concentration, flux, and membrane area, respectively; and the subscripts d, w, dd, c, and f are DS, water, diluted DS, concentrate, and FS, respectively.

In order to account for ICP and ECP in a full-scale PRO, the model boundary conditions in Figure 1 should be expressed with the operation parameters in Figure 2 such as:

$$c_5 = \frac{C_{\mathrm{d}} + C_{\mathrm{dd}}}{2} \tag{6}$$

$$c_1 = \frac{C_{\mathrm{f}} + C_{\mathrm{c}}}{2} \tag{7}$$

$$\Delta P = \frac{P_{\mathrm{d,\,in}} + P_{\mathrm{d,\,out}}}{2} - \frac{P_{\mathrm{f,\,in}} + P_{\mathrm{f,\,out}}}{2} \tag{8}$$

$$U_d = \left(Q_d + Q_{dd}\right)/\left(2\phi w H_d\right) \tag{9}$$

$$U_f = \left(Q_f + Q_c\right)/\left(2\phi w H_f\right) \tag{10}$$

Where, U, ϕ, w, and H are crossflow velocity, spacer porosity, channel width, and channel height, respectively; and the subscripts in and out are input and output, respectively.

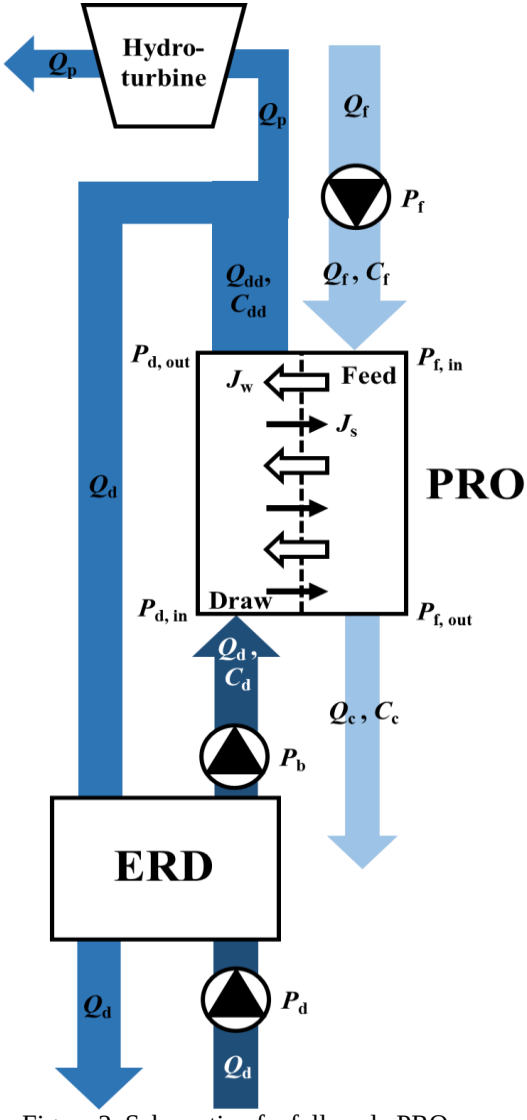

Figure 2. Schematic of a full-scale PRO process

2.3 Net energy analysis

In a full-scale PRO process such as Figure 2, the three pumps (DS, FS, and booster pumps) consume energy and the hydro-turbine produces energy. The power produced or consumed by these hydraulic devices can be expressed as the product of pressure and flow rate. Thus, the net power (W_{net}) produced from a full-scale PRO process can be expressed as:

$$W_{\text{net}} = W_{ht} - W_d - W_f - W_b \tag{11}$$

$$W_{ht} = P_{d,out} Q_p \eta_t \eta_g \tag{12}$$

$$W_d = P_d Q_d / (\eta_{p,d} \eta_{m,d}) \tag{13}$$

$$W_f = P_f Q_f / (\eta_{p,f} \eta_{m,f}) \tag{14}$$

$$W_b = P_b Q_d / (\eta_{p,b} \eta_{m,b}) \tag{15}$$

Where, W is the power produced or consumed by a hydraulic device; η_t, η_g, η_p, and η_m are the efficiencies of turbines, generators, pumps, and motors; and the subscripts ht, d, f, and b represent the hydro-turbine, DS supply pump, FS supply pump, and booster pump, respectively. In general, the efficiency of a hydraulic device is a function of the capacity of the device and the efficiencies becomes higher at larger capacities [12, 13]. The efficiencies of the DS, FS, and booster pump can be provided by Power model (Energy Recovery, Inc) by inputting a flow rate and pressure for a pump [14].

3 Results and discussions

Figure 3 shows membrane power density (MPD) in a typical hydrodynamic condition (DS inlet velocity = 0.035 m/s, FS inlet velocity = 0.076 m/s). MPD in the full-scale PRO is smaller than that in the lab-scale PRO because of the scale-up effect, which means that DS is diluted and FS is concentrated while both solutions flow through each channel.

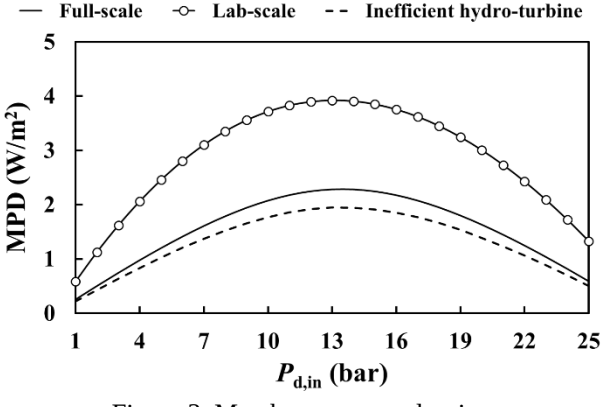

Figure 3. Membrane power density

If a realistic efficiency of a hydro-turbine is considered, the power density gained by the full-scale PRO should be decreased as shown in Figure 3, where the efficiencies of turbine (η_t) and generator (η_g) are assumed to be 0.87 and 0.98, respectively.

Figure 4 shows power consumed by the DS pump and power loss from the ERD and channels in the same operation condition as Figure 3. The power consumption of the DS pump remains constant because a constant inlet pressure is assumed. Power loss in the ERD increases at higher DS inlet pressures because a constant ratio of output pressure to input pressure of the ERD is assumed for the simulation. According to Equations (1) and (8), water flux in PRO decreases as DS inlet pressure increases. Thus, power loss from the FS channel pressure drop increases at higher DS inlet pressures because the crossflow velocity in the FS channel increases due to the decreased water flux. If water flux decreases, the diluted DS flow rate decreases and the crossflow velocity in the DS channel decreases. This is the reason why power loss from the DS channel pressure drop decreases at higher DS inlet pressure as shown in Figure 4.

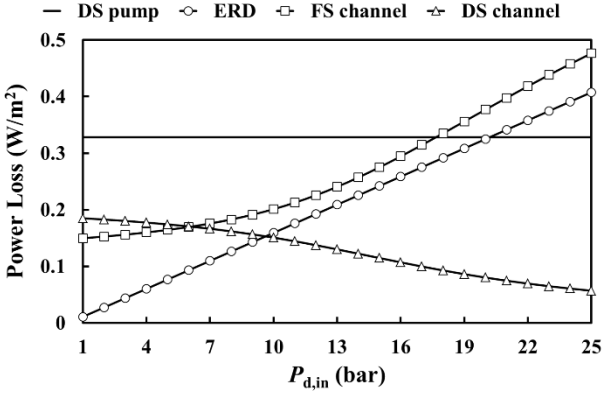

Figure 4. Power loss due to inefficient hydraulic devices and pressure drop

Figure 5 shows the net specific energy (NSE) produced from a full-scale PRO system under a typical hydrodynamic condition (Q_d = 50 m^3/d per module, Q_f = 55 m^3/d per module, $P_{d,in}$ = 15 bar). The plant capacity is defined as the sum of DS and FS inlet flow rates, and it is controlled by changing the number of PRO modules. The efficiencies of hydraulic devices (pumps and ERD) are obtained using Power model [14] and real ERD products (e.g., Pressure Exchanger, Energy Recovery, Inc.) are considered for the simulation. The efficiencies increase at larger plant capacities. For example, the smallest PRO system in Figure 5 uses pumps with efficiencies of 47–52 % and motors with efficiencies of 86–90%, while the largest system uses pumps with efficiencies of 88–89% and motors with efficiencies of 95–96%. In the case of the hydro-turbine, the efficiencies of the turbine and generator are assumed to be the same as those of the pump and motor. Since the efficiencies of hydraulic devices increases at larger plant capacities, the NSE increases as the plant capacity increases as shown in Fig. 5. The highest net energy

obtained from a full-scale PRO using seawater is 36.8 Wh/m^3 with 100,000 m^3/d of plant capacity, and the critical plant capacity to obtain the positive NSE is around 1,000 m^3/d.

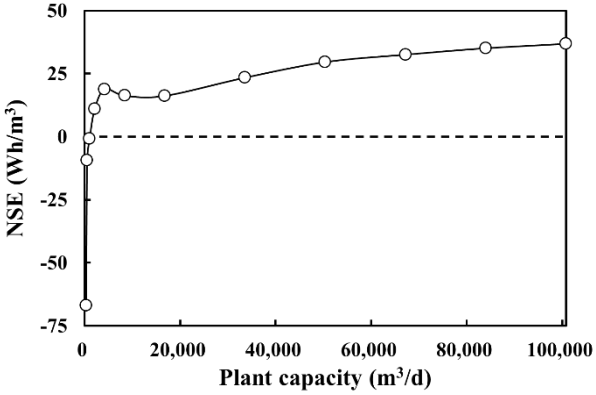

Figure 5. Net specific energy produced from a full-scale PRO system as a function of plant capacity

4 Conclusion

The ideal power potential of the osmotic gradient between seawater and fresh water is up to 4 W/m^2 with PRO membranes currently available under a realistic hydraulic condition. However, the actual power available from the PRO process using seawater and fresh water becomes much smaller than expected, and sometimes falls in the negative region. The scale-up effect (e.g., diluted DS and concentrated FS) and the inefficiency of hydraulic devices (e.g., pumps and ERDs) are found to be responsible for this discrepancy between the ideal and actual power potentials. The full-scale PRO simulation results reveal that we can obtain energy up to 36.8 Wh/m^3 from seawater using the full-scale PRO system over 1,000 m^3/d. Unfortunately, if the energy consumption for pretreating DS and FS (generally estimated around 200 Wh/m^3) is considered, it can be concluded that a full-scale PRO system cannot derive energy from the ocean.

Acknowledgements

This work was supported by the National Research Foundation of Korea (NRF) grant funded by the Korea government (MSIP; Ministry of Science, ICT & Future Planning) (No. 2017R1A2B4002990).

References

[1] A. P. Starub, S. Lin, M. Elimelech, "Module-scale analysis pressure retarded osmosis: performance limitations and implications for full-scale operation", *Environ. Sci. Technol.*, vol. 48, pp. 12435-12444, Oct. 2014.

[2] S. Loeb, R.S. Norman, "Osmotic power plants", *Science*, vol. 189, pp. 654–655, Aug. 1975.
[3] N. Y. Yip, M. Elimelech, "Thermodynamic and energy efficiency analysis of power generation from natural salinity gradients by pressure retarded osmosis", *Environ. Sci. Technol*, vol. 46, pp. 5230-5239, May. 2012.
[4] N. Y. Yip, M. Elimelech, "Performance limiting effects in power generation from salinity gradients by pressure retarded osmosis", *Environ. Sci. Technol*, vol. 45, pp. 10273-10282, Dec. 2011.
[5] N. Y. Yip, M. Elimelech, "Influence of natural organic matter fouling and osmotic backwash on pressure retarded osmosis energy production from natural salinity gradients", *Environ. Sci. Technol*, vol. 47, pp. 12607-12616, Nov. 2013.
[6] J. Lee, S. Kim, "Predicting power density of pressure retarded osmosis (PRO) membranes using a new characterization method based on a single PRO test", *Desalination*, vol. 389, pp. 224-234, Jul. 2016.
[7] J. Lee, J. Y. Choi, J.-S. Choi, K. H, Chu, Y. Yoon, S. Kim, "A statistics-based forward osmosis membrane characterization method without pressurized reverse osmosis experiment", *Desalination*, vol. 403, pp. 36-45, Feb. 2016.
[8] B. J. Feinberg, G. Z. Ramon, E. M. V. Hoek, "Scale-up characteristics of membrane-based salinity-gradient power production", *J. Membr. Sci*, vol. 476, pp. 311-320, Feb. 2015.
[9] S.H. Park, B. Park, H.K. Shon, S. Kim, "Modeling full-scale osmotic membrane bioreactor systems with high sludge retention and low salt concentration factor for wastewater reclamation", *Bioresour. Technol*, vol. 190, pp. 508–515, Aug. 2015.
[10] S. Kim, "Scale-up of osmotic membrane bioreactors by modeling salt accumulation and draw solution dilution using hollow-fiber membrane characteristics and operation conditions", *Bioresour. Technol*, vol. 165, pp. 88–95, Aug. 2014.
[11] S. Kim, H. Park, "Applicability Assessment of Sub-critical Flux Operation in Crossflow Microfiltration By Modeling and Experiment", *J. Environ. Eng*, vol. 128 (4), pp. 335-340, Apr. 2002.
[12] W. He, Y. Wang, I. M. Mujtaba, M. H. Shaheed, "An evaluation of membrane properties and process characteristics of a scaled-up pressure retarded osmosis (PRO) process", *Desalination*, vol. 378, pp. 1-13, Jan. 2016.
[13] A. D. Karlis, D. P. Papadopoulos, "A systematic assessment of the technical feasibility and economic viability of small hydroelectric system installations", *Renewable Energy*, vol. 20, pp. 253-262, Jun. 2000.
[14] Energy Recovery, Inc., Webpage, http://www.energyrecovery.com

10TH INTERNATIONAL CONFERENCE ON SUSTAINABLE ENERGY AND ENVIRONMENTAL PROTECTION (JUNE 27TH – 30TH, 2017, BLED, SLOVENIA), MARINE AND HYDRO POWER
J. Krope, A.Ghani Olabi, D. Goričanec & S. Božičnik

University of Maribor Press

High Resolution 3D Modelling of the Swansea Bay Tidal Lagoon

NEJC ČOŽ, REZA AHMADIAN & ROGER A FALCONER

Abstract Increasing awareness of Climate Change and the rising price of fossil fuels have resulted in a rapid growth in demand for various types of renewable energy, including tidal energy. To date only a few small scale tidal schemes are in operation worldwide. One of the most attractive sites for the deployment of tidal range schemes is along the UK Bristol Channel and Severn Estuary. This region experiences the second largest tidal range in the world, often exceeding 10 m in the basin. This paper investigates the impacts of the proposed tidal lagoon in Swansea Bay. Previous studies have highlighted the potential significance of momentum conservation when modelling the outflowing jet from the turbines. Therefore, this study focuses on accurate representation of the turbines and maintaining momentum conservation. Here a finite difference method was used for the hydraulic simulations, and the momentum associated with the flow through the turbines was represented as an additional term in the momentum equation. Simulations were performed both in 2D and 3D. A noticeable difference was observed in the velocity profile predicted by the two models in close proximity to the turbines, highlighting the importance of implementing a more detailed 3D model.

Keywords: • Tidal Lagoon • Swansea Bay • Marine Renewable Energy • Hydraulic Structures • Delft3D •

CORRESPONDENCE ADDRESS: Nejc Čož, PhD student, Cardiff University, School of Engineering, Hydro-environmental Research Centre, Queen's Buildings, 14-17 The Parade, Cardiff CF24 3AA, UK, e-mail: CozN@cardiff.ac.uk. Reza Ahmadian, Ph.D., Cardiff University, School of Engineering, Hydro-environmental Research Centre, Queen's Buildings, 14-17 The Parade, Cardiff CF24 3AA, UK, e-mail: AhmadianR@cardiff.ac.uk. Roger A Falconer, Ph.D., Professor, Cardiff University, School of Engineering, Hydro-environmental Research Centre, Queen's Buildings, 14-17 The Parade, Cardiff CF24 3AA, UK, e-mail: FalconerRA@cardiff.ac.uk.

https://doi.org/10.18690/978-961-286-055-4.5 ISBN 978-961-286-055-4

Available at: http://press.um.si.

1 Introduction

The demand for renewable energy is developing rapidly. Although there is an increased interest in harvesting tidal power, only a few small-scale working tidal power plants are currently in operation world-wide. Places where tidal energy has the most potential are areas with a large tidal range, i.e. where the difference between low and high water levels is large enough to create a sufficient head difference to produce energy. One such place is in the Bristol Channel and Severn Estuary in the UK, where there is an exceptional tidal range, particularly in the Severn Estuary.

Swansea Bay is one of the most attractive sites for the deployment of a tidal range pilot study. The Swansea Bay tidal lagoon project recently received a backing from Charles Hendry's independent review [1] confirming its viability and paving the way towards the construction of the first tidal energy project in the estuary in the very near future. Other similar tidal schemes can be expected to follow.

The study area is situated on the southern coast of Wales and is located in the Bristol Channel (Figure 1). Together with the Severn Estuary, this body of water experiences the second largest tidal range in the world, often exceeding 10 m during spring tides. Although relatively small in scale, Swansea Bay Lagoon will become the largest tidal range power plant ever constructed. With an installed capacity of 320 MW it would overtake the tidal barrages at La Rance in France and Sihwa in South Korea, with installed capacities of 240 MW and 254 MW respectively [1].

Figure 1. Computational domain overlaid over the Severn Estuary and Bristol Channel.

This study focuses on the correct representation of the tidal lagoon in a hydrodynamic model. The model Delft3D-FLOW was used for solving the hydrodynamic equations, with modifications made to the source code to allow for correct mass and momentum conservation of the discharge through the turbines and sluices gates. Both the 2D shallow

water and 3D Navier-Stokes simulations were refined and studies, illustrating the importance of detailed modelling of complex flows in the vicinity of turbines.

2 Methodology

2.1 Governing equations

This study employed both the 2D shallow water equations and the 3D sigma-layer equations. In the 2D case a depth averaged approach is used and the continuity equation is solved, together with the two momentum equations (1) and (2) in the horizontal plane. For a 3D simulation a third momentum equation (3) is added in the vertical direction.

$$\frac{\partial u}{\partial t}+\frac{u}{\sqrt{G_{\xi\xi}}}\frac{\partial u}{\partial \xi}+\frac{u}{\sqrt{G_{\eta\eta}}}\frac{\partial u}{\partial \eta}+\frac{\omega}{d+\varsigma}\frac{\partial u}{\partial \sigma}-\frac{v^2}{\sqrt{G_{\xi\xi}}\sqrt{G_{\eta\eta}}}\frac{\partial\sqrt{G_{\eta\eta}}}{\partial \xi}+\frac{uv}{\sqrt{G_{\xi\xi}}\sqrt{G_{\eta\eta}}}\frac{\partial\sqrt{G_{\xi\xi}}}{\partial \eta}-f_v=$$
$$-\frac{1}{\rho_0\sqrt{G_{\xi\xi}}}P_\xi+F_\xi+\frac{1}{(d+\varsigma)^2}\frac{\partial}{\partial\sigma}\left(\nu_V\frac{\partial u}{\partial\sigma}\right)+M_\xi \quad (1)$$

$$\frac{\partial v}{\partial t}+\frac{u}{\sqrt{G_{\xi\xi}}}\frac{\partial v}{\partial \xi}+\frac{u}{\sqrt{G_{\eta\eta}}}\frac{\partial v}{\partial \eta}+\frac{\omega}{d+\varsigma}\frac{\partial v}{\partial \sigma}-\frac{uv}{\sqrt{G_{\xi\xi}}\sqrt{G_{\eta\eta}}}\frac{\partial\sqrt{G_{\eta\eta}}}{\partial \xi}+\frac{u^2}{\sqrt{G_{\xi\xi}}\sqrt{G_{\eta\eta}}}\frac{\partial\sqrt{G_{\xi\xi}}}{\partial \eta}-f_u=-\frac{1}{\rho_0\sqrt{G_{\eta\eta}}}P_\eta+$$
$$F_\eta+\frac{1}{(d+\varsigma)^2}\frac{\partial}{\partial\sigma}\left(\nu_V\frac{\partial v}{\partial\sigma}\right)+M_\eta \quad (2)$$

$$w=\omega+\frac{1}{\sqrt{G_{\xi\xi}}\sqrt{G_{\eta\eta}}}\left[u\sqrt{G_{\eta\eta}}\left(\sigma\frac{\partial H}{\partial\xi}+\frac{\partial\varsigma}{\partial\xi}\right)+v\sqrt{G_{\xi\xi}}\left(\sigma\frac{\partial H}{\partial\eta}+\frac{\partial\varsigma}{\partial\eta}\right)\right]+\left(\sigma\frac{\partial H}{\partial t}+\frac{\partial\varsigma}{\partial t}\right) \quad (3)$$

where u, v and ω are the flow velocities in ξ, η and σ direction respectively, w is the fluid velocity in the z direction, f_u and f_v are the Coriolis parameters, ν_V is the vertical eddy viscosity, P_ξ and P_η are the pressure gradients, forces F_ξ and F_η represent the imbalance of the horizontal Reynold's stresses, M_ξ and M_η represent the contributions due to external sources or sinks of momentum and $\sqrt{G_{\xi\xi}}$ and $\sqrt{G_{\eta\eta}}$ are used for transformation of the coordinate system.

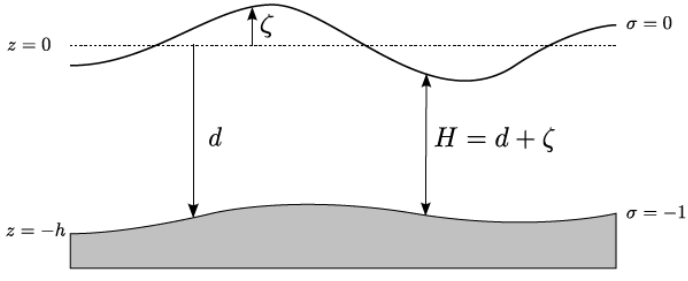

Figure 2. Definition of water level (ς), depth (d) and total depth (H) for the sigma-model [2].

The contribution of the discharge through turbines and sluice gates is represented by the terms M_ξ and M_η in the momentum equations and is implemented in a similar way as for the momentum sink terms in [3].

The domain of a 3D model is divided into many layers (planes), which are not strictly horizontal but follow the shape of the bottom topography and free surface. Instead of a fixed layer depth, the sigma-layers are characterized by the proportion of the total depth (Figure 3).

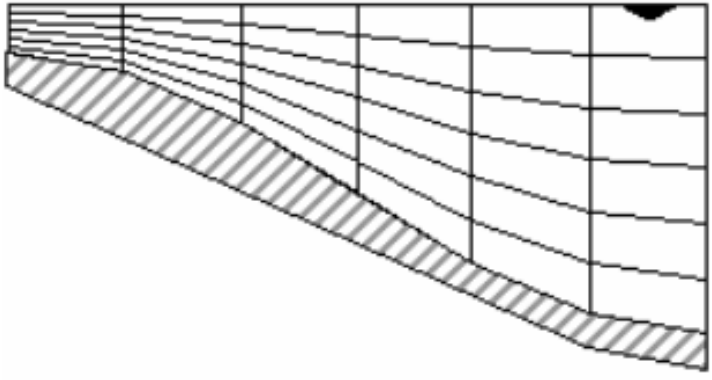

Figure 3. Example of the sigma grid.

The simulations were conducted using the Delft3D-FLOW, a hydrodynamic module of the Delft3D software suite, developed by Deltares in the Netherlands. A curvilinear staggered grid is used for the discretization of the partial differential equations which are solved using a finite difference altering direction implicit (ADI) solver to provide a second order accurate solution of the equations [2].

2.2 Modification of turbines and sluice gates

The open source aspect of the Delft3D suite is an important advantage as it allows the user to modify the code to better fit the requirements of an individual study. In the simulations presented herein the code was modified to represent the operation of tidal range structures (TRS) by including turbines and sluice gates. They are both represented as culverts, however the discharge between the inlet and outfall is calculated differently for each of the structures. With turbines the discharge is calculated from a "Hill chart" (Figure 4), whereas a standard orifice equation (Eq. 4) is used for the sluice gates.

$$Q = c_d A\sqrt{2gH} \tag{4}$$

Furthermore, the code was modified to simulate the operation of the lagoon based on the head difference of the water surface levels upstream and downstream of the lagoon. A

discharge through the turbines is only allowed when the head difference exceeds the driving head of the turbines. If the head falls below the minimal efficient head then the turbines are stopped and sluicing is initiated. Once the water levels on both sides are nearly equal, i.e. the head difference falls close to zero, then both the turbines and sluice gates are closed.

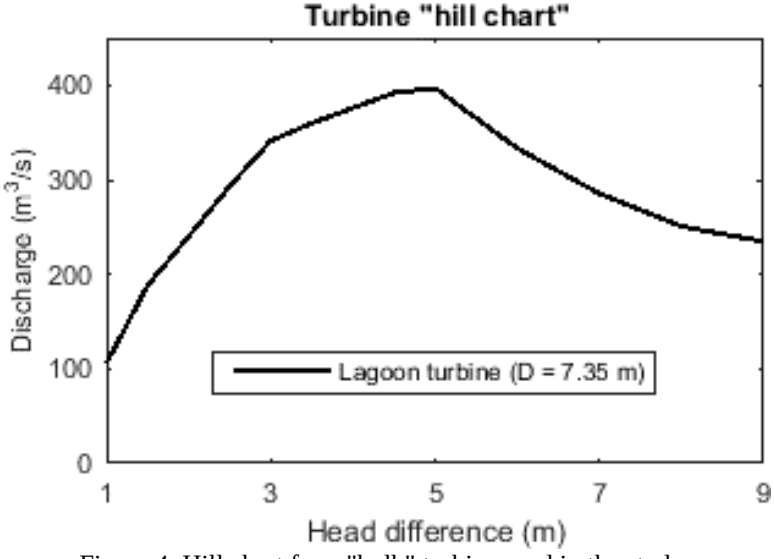

Figure 4. Hill chart for a "bulb" turbine used in the study.

2.3 Swansea Bay Lagoon Model

The idea for a tidal lagoon in Swansea Bay has been around for more than a decade. In this period there have been numerous project proposals with different lagoon layouts and turbine capacities. In 2015 a project by Tidal Lagoon Plc received a development consent order (DCO) from the UK government [1]. Their most current scheme proposes a 9.5 km long embankment that would form an impoundment with a surface area of 11.5 km^2 [4]. The potential installed capacity of 320 MW would be achieved through a set of sixteen bulb turbines, each with a diameter of 7.35 m and an output power of 20 MW. The same characteristics are also being used in other recent studies, such as Ref. [5]–[7]. A total sluice gate area of 800 m^2 is assumed.

The extent of the model domain is shown in Figure 1. The computational grid covers the Bristol Chanel and Severn Estuary. The size of the computational cells range from more than 400 m at the seaward boundary, to 100 m in the areas around the lagoon. The open boundary, located at the entrance to the Bristol Chanel, stretches from Heartland Point in south west England, to the southwest tip of Pembrokeshire in Wales. The model was validated against the ADCP measurements during a typical 14 day neap-spring tidal cycle, from 25/7/2012 to 7/8/2012.

For simplicity, validation results are shown only for one of the observation points, located in Swansea Bay and in the vicinity of the lagoon (Figures 5 and 6). The whole domain has been validated in a similar manner and the same level of agreement between both sets of predicted and measured results was observed throughout the domain.

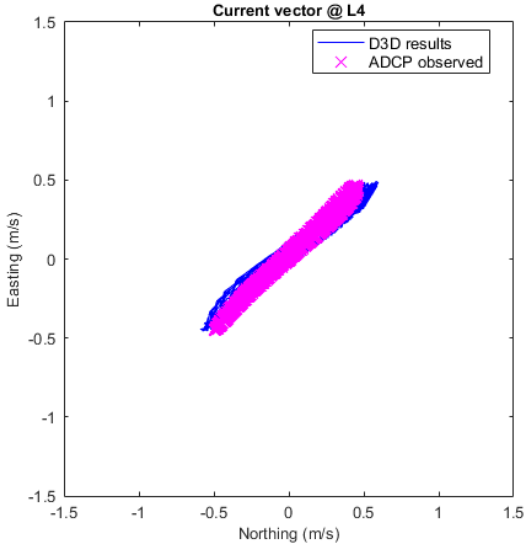

Figure 5. Calibration - velocity vectors, showing the magnitude and direction of the flow.

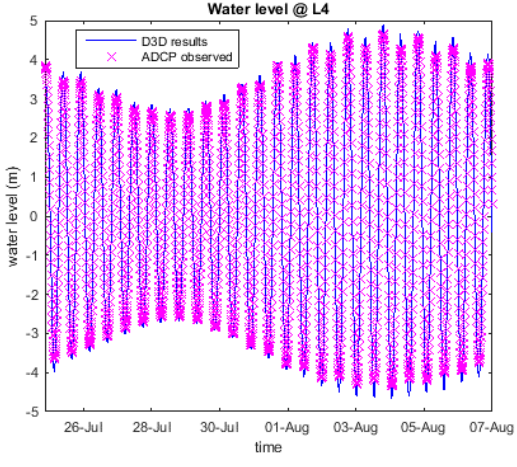

Figure 6. Calibration – comparison of calculated and measured water levels.

3 Results And Discussion

3.1 Operation of the lagoon

The operation of the lagoon can be illustrated with a time series of water levels observed on the inside and outside of the lagoon. Figure 7 shows a 24-hour period during a typical spring tide. The model was set up for "two-way" operation, where energy is generated during both ebb and flood tides. Taking into account the trigger conditions explained in section 2.2, the operation sequence of the lagoon can be split into six distinctive phases [6]:

a) Holding high water – water outside is receding and inside retained at high level, turbines are closed;
b) Generating – ebb flow, turn on the turbines when sufficient head difference is established, water surface level both outside and inside is falling
c) Releasing – when the head difference falls below minimal head stop generating, open sluice gates
d) Holding low water – water outside is rising, inside retained at low level, turbines are closed
e) Generating – flood flow, turn on the turbines when sufficient head difference is established, water surface level both outside and inside is rising
f) Filling – when the head difference falls below minimal head stop generating, open sluice gates

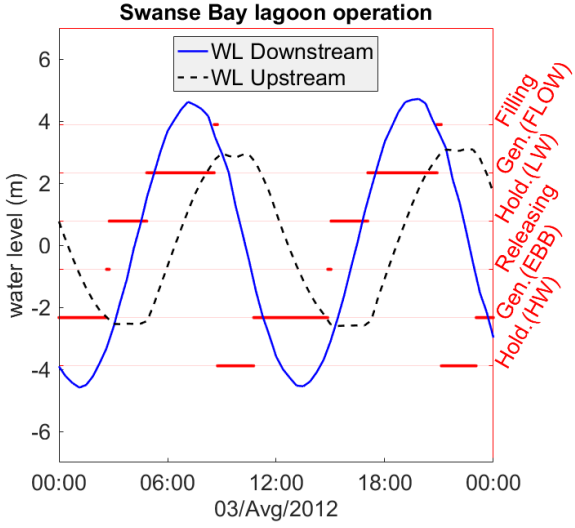

Figure 7. Lagoon operation and water levels downstream and upstream of the turbines during a typical spring cycle.

3.2 Velocities – turbine wake

The velocities illustrated in Figures 8a and 8b correspond to the maximum turbine flow rate during ebb generation, for the 2D and 3D models respectively. The contour plots, overlain with velocity vectors, enable both the magnitude and direction of the flow to be observed. For better comparisons, the magnitude of the 2D results was subtracted from the 3D results and plotted on Figure 8c.

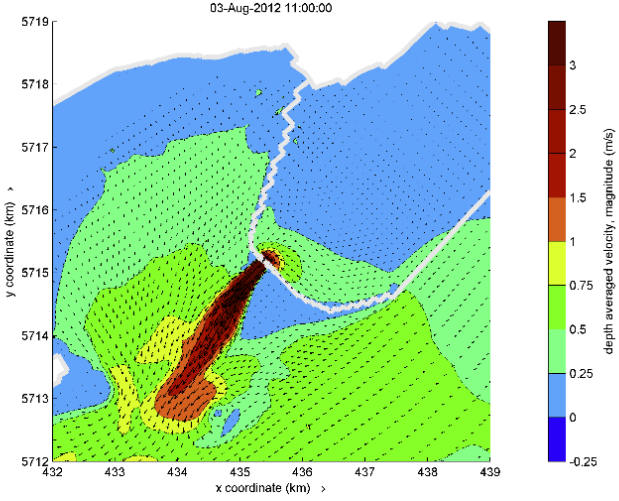

a) 2D, depth av. velocity (m/s)

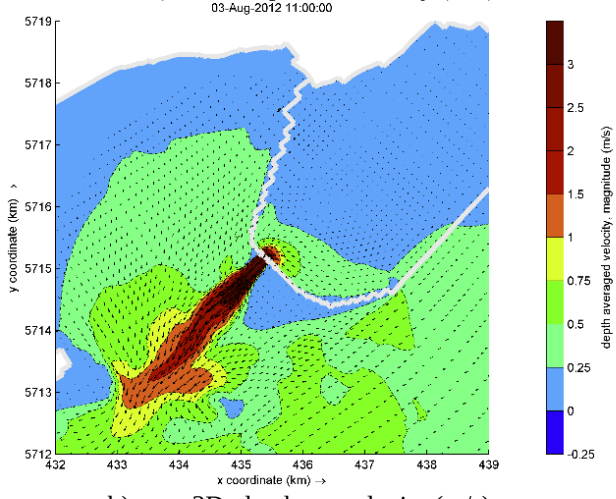

b) 3D, depth av. velocity (m/s)

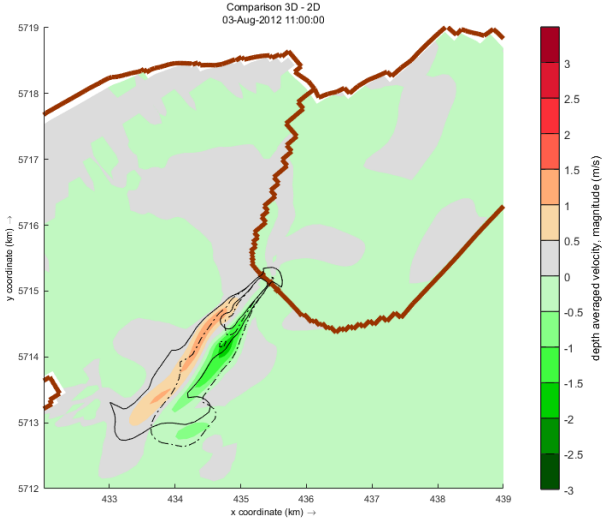

c) 3D vs 2D, magnitude (m/s)

Figure 8. Turbine wakes: a) 2D, depth averaged results; b) 3D results, subsequently depth averaged for comparison; c) difference in the magnitude between the two.

The results illustrate that a 3D model is preferable for simulating complex velocity fields, such as those occurring in turbine wakes. Although both models predict a wake of similar length, there are several distinct differences that can be observed. For instance, the wake spreads over a wider distance with the 3D simulations, while the 2D run predicts a narrower jet. This can be clearly seen in Figure 8c where the solid and "dash-dot" lines present the 1 m/s contour for the 2D and 3D results respectively.

The formation of a counter-rotating recirculation zone can be spotted adjacent to the turbine wake. It is formed due to the positioning of the turbines in a relatively narrow section of the lagoon. The 2D simulation shows slightly higher velocities in the recirculation zone, which is consistent with the findings from [8], where 2D models showed a considerable increase in the prediction of the velocity in the recirculation zone caused by flows around headlands.

3.3 Velocity profiles

The turbines and sluice gates are fully submerged under water. The vertical elevation of their intakes and outfalls was assumed to be at 7m below ordnance datum. This detail has no effect on the 2D depth averaged model, as any discharge added to the computation is evenly distributed over the height of the computational cell. However, it has a significant

effect in the 3D model, where the discharge can be concentrated in a single vertical layer and thus more accurately representing the complexity of the out coming jet.

It can be seen that the layer where the turbine outfall is located has a considerably higher velocity than others. Consequentially, the average of the velocities of the five layers becomes relatively higher than the depth averaged velocity obtained from the 2D model. The discrepancy between the two sets of results can lead to unrealistic predictions of the bottom shear stress, which can therefore have a significant impact on bed load transport.

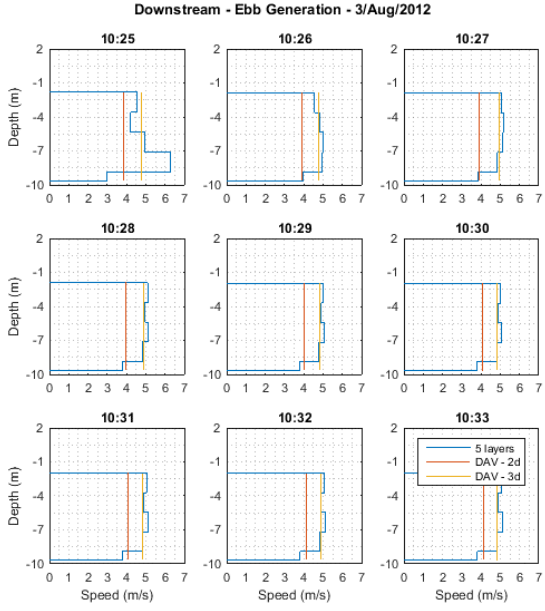

Figure 9 illustrates the difference between the depth averaged and 3D approaches.

4 Conclusions

In this paper, 2D and 3D hydraulic numerical models for Swansea Bay lagoon were compared and the instantaneous velocity field during the power generation of the lagoon was investigated. The results show the advantages of a 3D model when simulating complex flows, such as those generated through turbine wakes. A distinctive recirculation zone was observed as a result of the high velocity jet. The 2D model slightly over predicted the intensity of the recirculation zone, which is consistent with the findings from the literature.

In the current study a 3D model with 5 vertical layers was used. For future studies a 3D model with a larger number of layers will be considered, with thinner layers at the bottom, to better capture the complex flow patterns during the generation phases.

Acknowledgements

The research reported herein is funded by The Engineering and Physical Sciences Research Council (EP/L016214/1) and is part of a PhD research topic at Centre for Doctoral Training in Water Informatics: Science and Engineering (WISE CDT).

References

[1] C. Hendry, "The role of tidal lagoons," 2016.
[2] Deltares, "Delft3D-FLOW, User Manual," pp. 1–684, 2014.
[3] R. Ahmadian, R. Falconer, and B. Bockelmann-Evans, "Far-field modelling of the hydro-environmental impact of tidal stream turbines," *Renew. Energy*, vol. 38, no. 1, pp. 107–116, 2012.
[4] "Key Statistics - Tidal Lagoon." [Online]. Available: http://www.tidallagoonpower.com/projects/swansea-bay/key-statistics/. [Accessed: 19-Apr-2017].
[5] A. Angeloudis and R. A. Falconer, "Sensitivity of tidal lagoon and barrage hydrodynamic impacts and energy outputs to operational characteristics," *Renew. Energy*, no. August, 2016.
[6] A. Angeloudis, R. A. Falconer, S. Bray, and R. Ahmadian, "Representation and operation of tidal energy impoundments in a coastal hydrodynamic model," *Renew. Energy*, vol. 99, pp. 1103–1115, 2016.
[7] S. Petley and G. Aggidis, "Swansea Bay tidal lagoon annual energy estimation," *Ocean Eng.*, vol. 111, pp. 348–357, 2016.
[8] P. Stansby, N. Chini, and P. Lloyd, "Oscillatory flows around a headland by 3D modelling with hydrostatic pressure and implicit bed shear stress comparing with experiment and depth-averaged modelling," *Coast. Eng.*, vol. 116, pp. 1–14, 2016.


METTLER TOLEDO
PRINSIS
energetika ljubljana